August 10, 1990

HADRON SUPERCOLLIDERS: THE 1-TEV SCALE AND BEYOND *

Lectures presented at the Workshop/Symposium on TeV Physics
China Center of Advanced Science and Technology
Beijing, May 28 - June 8, 1990

Chris Quigg

Theoretical Physics Group
Physics Division
Lawrence Berkeley Laboratory
1 Cyclotron Road
Berkeley, California 94720

HADRON SUPERCOLLIDERS: THE 1-TEV SCALE AND BEYOND

CHRIS QUIGG

Lawrence Berkeley Laboratory, Berkeley, CA 94720 USA

Abstract Greater understanding of the connection between the weak and electromagnetic interactions is central to progress in elementary-particle physics. A definitive exploration of the mechanism for electroweak symmetry breaking will require collisions between fundamental constituents at energies on the order of 1 TeV. This goal drives the design of high-energy, high-luminosity hadron colliders that will be commissioned during the next decade, but by no means completely defines their scientific potential. These three lectures are devoted to a review of the standard-model issues that motivate an experimental assault on the 1-TeV scale, an introduction to the machines and the experimental environment they will present, and a survey of possibilities for measurement and discovery with a multi-TeV hadron collider.

INTRODUCTION

What will be the physics of the next generation of great accelerators, the proton-proton colliders that will allow us for the first time to explore constituent interactions at energies of 1 TeV and beyond? During the course of this symposium, we shall be able to give a series of detailed—but certainly incomplete—answers. My aim in these lectures is to develop the question broadly and to survey some of the possible outcomes. There is no reason to believe that important discoveries at TeV energies will be limited to what we have already imagined, though that is itself a very long list indeed[1-13].

When we contemplate the searches and measurements to be carried out, we must pay attention to the conditions under which detectors must operate, the information that will be required to address important questions, and the backgrounds that can obscure the desired signal or confound its interpretation. These

practical matters will be implicit in everything I have to say, but will receive particular attention in the second lecture. Theorists need to be disciplined by reality, just as experimenters do, and should have something to contribute to the discussion of which future experiments may be both practical and worthwhile. We should therefore have in mind from the start the characteristics of the machines on the horizon, which are high-energy, high-luminosity, proton-proton colliders. The Superconducting Super Collider (SSC) project is getting under way in the United States, near Dallas. A decision may be made within about two years on whether to construct a Large Hadron Collider (LHC) in the LEP tunnel at CERN. The current design goals for both these machines are shown in Table I.

TABLE I   Design parameters of future proton-proton colliders.

Machine	$\sqrt{s}$ [TeV]	Peak Luminosity [$cm^{-2}s^{-1}$]	Magnetic Field [T]
SSC	40	10^{33}	6.6
LHC	16	$3 \cdot 10^{34}$	10

Each of these supercolliders is quite adventurous in its own way, but the philosophies underlying the two designs are very different. The SSC design emphasizes very high energy, so that much of the initial physics program we contemplate can be accomplished with a luminosity of 10^{32} $cm^{-2}s^{-1}$, a regime in which multipurpose detectors should be able to operate gracefully. Higher luminosities—perhaps up to $2 \cdot 10^{34}$ at 37 TeV—are available as detectors and scientific questions mature. The LHC design emphasizes very high luminosity, to exploit the advantages of an existing tunnel whose size limits the beam energy to about 0.8 TeV per tesla. In either machine, the high rate of complicated, high-multiplicity events challenges the detector builder to accomplish what would have been unthinkable only a short time ago.

The picture of the fundamental constituents of matter and the interactions among them that has emerged in recent years is one of great beauty and simplicity. All matter appears to be composed of quarks and leptons, which are point-

like, structureless, spin-$\frac{1}{2}$ particles. If we leave aside gravitation, which is a negligible perturbation at the energy scales usually considered, the interactions among these particles are of three types: weak, electromagnetic, and strong. All three of these interactions are described by gauge theories and are mediated by spin-1 gauge bosons. The quarks experience all three interactions; the leptons participate only in the weak and electromagnetic interactions. By the standard model we will understand two elements: the $SU(3)_c \otimes SU(2)_L \otimes U(1)_Y$ gauge theory of the strong, weak, and electromagnetic interactions; and three generations of color-triplet quarks ($u, d, s, c, b, [t]$), and color-singlet leptons (e, $v_e, \mu, v_\mu, \tau, [v_\tau]$). (We know that the top quark must exist, because[14] the b-quark has weak isospin $I_3 = -\frac{1}{2}$, and that its mass is likely[15] to be less than 250 GeV/c^2, but it has so far eluded detection. The most restrictive limit, on the assumption than $t \rightarrow b + W^+$ is a prominent decay mode, comes from the CDF collaboration: $m_t > 89$ GeV/c^2 at 95% confidence level[16]. A three-neutrino experiment that would confirm the existence of the tau-neutrino has never been carried out.) With its appealing simplicity and impressive generality, the standard model holds the promise of deeper understanding—in the form of a further unification of the interactions—still to come.

ELECTROWEAK SYMMETRY BREAKING AND THE HIGGS BOSON

Much of the impulse for a large increase in collider energy comes simply from the desire to open up a vast new territory for measurement, search, and discovery. Many of the phenomena for which we would search do not have a known energy scale. However, one problem that seems particularly acute does select a range of energies—constituent scattering energies around 1 TeV—as the regime in which answers are to be found. That problem—the nature of electroweak symmetry breaking—is so important that we take it as the starting point for our discussion of supercollider physics.

In simplest terms, the question is this: why does electromagnetism act over astronomical distances (i.e., have infinite range) when the weak interactions to which it is related by gauge symmetry act only over distances smaller

than 10^{-15} cm? More generally, as we shall see, the issue is the origin of mass—for the quarks and leptons as well as the gauge bosons.

The standard model is treated in many textbooks[17-18]. A quick tour is nevertheless in order, if only to ensure that we use a common language and notation.

We will confine our attention in this first lecture to the standard electroweak theory. It is built upon three quark and lepton generations that transform under $SU(2)_L \otimes U(1)_Y$ as

$$\begin{pmatrix} u \\ d_\theta \end{pmatrix}_L \qquad u_R, d_R \qquad Y_L = 1/3; Y_R = \begin{pmatrix} 4/3 \\ -2/3 \end{pmatrix}$$

$$, \quad (1)$$

$$\begin{pmatrix} \nu_e \\ e \end{pmatrix}_L \qquad e_R \qquad Y_L = -1; Y_R = -2$$

where the weak-isospin and weak-hypercharge assignments guarantee that the Gell-Mann–Nishijima formula

$$Q = I_3 + \frac{1}{2} Y \qquad (2)$$

yields the appropriate charges. The electroweak gauge group implies two sets of gauge bosons: a weak isovector $\vec{b}_\mu$, with coupling constant g, and a weak-isoscalar a_μ, with coupling constant $g'/2$. Corresponding to these gauge fields are the field-strength tensors $\vec{F}_{\mu\nu}$ for the weak-isospin symmetry and $f_{\mu\nu}$ for the weak-hypercharge symmetry.

We may summarize the interactions by the Lagrangian

$$\mathcal{L} = \mathcal{L}_{gauge} + \mathcal{L}_{leptons} + \mathcal{L}_{quarks} \quad , \qquad (3)$$

where

$$\mathcal{L}_{gauge} = -\frac{1}{4} F^l_{\mu\nu} F_l^{\mu\nu} - \frac{1}{4} f_{\mu\nu} f^{\mu\nu}, \qquad (4)$$

$$\mathcal{L}_{leptons} = \bar{R} i\gamma^\mu \left(\partial_\mu + i\frac{g'}{2} a_\mu Y \right) R + \bar{L} i\gamma^\mu \left(\partial_\mu + i\frac{g'}{2} a_\mu Y + i\frac{g}{2} \vec{\tau} \cdot \vec{b}_\mu \right) L, \qquad (5)$$

with $R = e_R$ and $L = \begin{pmatrix} \nu_e \\ e \end{pmatrix}$. $\mathscr{L}_{quarks}$ has the same structure as $\mathscr{L}_{leptons}$, with separate terms for u_R and d_R, and with $L_q = \begin{pmatrix} u \\ d_\theta \end{pmatrix}$.

To hide the electroweak gauge symmetry $SU(2)_L \otimes U(1)_Y \to U(1)_{em}$, we introduce a complex doublet of scalar fields

$$\phi = \begin{pmatrix} \phi^+ \\ \phi^0 \end{pmatrix} \tag{6}$$

with weak hypercharge $Y_\phi = +1$. Its complex conjugate is the $SU(2)_L$ doublet

$$\bar{\phi} = i\,\sigma_2\,\phi^* = \begin{pmatrix} \bar{\phi}^0 \\ -\phi^- \end{pmatrix} \tag{7}$$

with $Y_{\bar{\phi}} = -1$. We add to the Lagrangian new terms for the interaction and propagation of the scalars,

$$\mathscr{L}_{scalar} = (\mathcal{D}^\mu \phi)^\dagger (\mathcal{D}_\mu \phi) - V(\phi^\dagger \phi), \tag{8}$$

where the gauge-covariant derivative is

$$\mathcal{D}_\mu = \partial_\mu + i\frac{g'}{2}a_\mu Y + i\frac{g}{2}\vec{\tau}\cdot\vec{b}_\mu, \tag{9}$$

and the potential has the form

$$V(\phi^\dagger \phi) = \mu^2(\phi^\dagger \phi) + |\lambda|(\phi^\dagger \phi)^2. \tag{10}$$

We are also free to add Yukawa interactions between the scalar fields and the fermions. The most general form (with a massless neutrino) is

$$\mathscr{L}_{Yukawa} = - G_e[\bar{R}(\phi^\dagger L) + (\bar{L}\phi)\,R] - G_u[\bar{u}_R(\phi^\dagger L_q) + (\bar{L}_q\phi)u_R] \tag{11}$$
$$- G_d[\bar{d}_R(\phi^\dagger L_q) + (\bar{L}_q\phi)d_R].$$

The electroweak symmetry is spontaneously broken if the parameter $\mu^2 < 0$. The minimum energy, or vacuum state, may be chosen to correspond to the vacuum expectation value

$$<\phi>_0 = \begin{pmatrix} 0 \\ v/\sqrt{2} \end{pmatrix}, \tag{12}$$

where $v = \sqrt{-\mu^2/|\lambda|} = (G_F\sqrt{2})^{-1/2} \approx 246$ GeV is fixed by the low-energy phenomenology of charged-current interactions.

Spontaneous symmetry breaking has several important consequences. The Yukawa interactions generate masses for the electron and for the up and down quarks. Three of the scalars become longitudinal components of weak gauge bosons. In this way, the charged weak bosons acquire mass

$$M_{W^\pm} = gv/2 \ . \tag{13}$$

The neutral weak boson

$$Z_\mu = \frac{-g' a_\mu + g b^3_\mu}{\sqrt{g^2 + g'^2}} \tag{14}$$

acquires mass

$$M_Z = \sqrt{g^2 + g'^2} \ v/2 \ . \tag{15}$$

The orthogonal combination

$$A_\mu = \frac{g a_\mu + g' b^3_\mu}{\sqrt{g^2 + g'^2}} \ , \tag{16}$$

which couples to electric charge, remains massless. To identify A_μ as the photon, we must fix its coupling to the electron as

$$\frac{g g'}{\sqrt{g^2 + g'^2}} = e \ . \tag{17}$$

With the definitions

$$\frac{g'}{\sqrt{g^2 + g'^2}} = \sin\theta_W \ , \quad \frac{g}{\sqrt{g^2 + g'^2}} = \cos\theta_W \ , \quad x_W = \sin^2\theta_W \tag{18}$$

we have

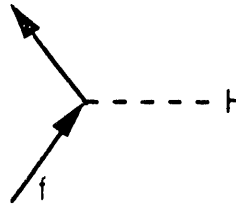$$g = e/\sin\theta_W \ , \quad g' = e/\cos\theta_W \ , \tag{19}$$

so that

$$M_W^2 = g^2/4G_F\sqrt{2} = e^2/4G_F\sqrt{2}\,x_W$$

$$M_Z^2 = M_W^2/(1 - x_W) \ . \tag{20}$$

While the standard model shows how fermion masses could arise through spontaneous symmetry breaking as $m_e = G_e\,v/\sqrt{2}$, etc., there is no prediction of the Yukawa couplings (hence the masses). Similarly, the mass of the physical Higgs boson is given in terms of unknown parameters of the Lagrangian as

$$M_H^2 = -2\mu^2 > 0 \ . \tag{21}$$

Because of its role in generating mass, the Higgs boson coupling to fermions is just

$$\frac{-iG_f}{\sqrt{2}} = \frac{-im_f}{v} = -im_f\,(G_F\sqrt{2})^{1/2} \ . \tag{22}$$

This is the standard path to the (theoretical) discovery of the Higgs boson and its properties. There is an important independent argument that assures us that—in any acceptable theory—something like the Higgs boson must exist. Consider the role of the Higgs boson in the cancellation of high-energy divergences. An illuminating example is provided by the reaction

$$e^+e^- \rightarrow W^+W^- \ , \tag{23}$$

which is described in lowest order in the Weinberg-Salam theory by the four Feynman graphs in Figure 1. The leading divergence in the $J=1$ amplitude of the neutrino-exchange diagram in Figure 1(a) is cancelled by the contributions of the direct-channel γ- and Z^0-exchange diagrams of Figures 1(b) and (c).

However, the $J=0$ scattering amplitude, which exists in this case because the electrons are massive and may therefore be found in the "wrong" helicity state, grows as $\sqrt{s}$ for the production of longitudinally polarized gauge bosons. The resulting divergence is precisely cancelled by the Higgs boson graph of Figure 1(d). If the Higgs boson did not exist, we should have to invent something very much like it. From the point of view of S-matrix theory, the Higgs-electron-electron coupling must be proportional to the electron mass, as in (22), because "wrong helicity" amplitudes are always proportional to the fermion mass.

Let us summarize: Without spontaneous symmetry breaking in the standard model, there would be no Higgs boson, no longitudinal gauge bosons, and no extreme divergence difficulties. (Nor would there be a viable low-energy phenomenology of the weak interactions.) The most severe divergences are eliminated by the gauge structure of the couplings among gauge bosons and leptons. A lesser, but still potentially fatal, divergence arises because the electron has acquired mass—because of the Higgs mechanism. Spontaneous symmetry breaking provides its own cure by supplying a Higgs boson to remove the last divergence. A similar interplay and compensation must exist in any satisfactory theory[19].

HIGGS BOSON PROPERTIES

We have already remarked that the standard model does not give a precise prediction for the mass of the Higgs boson. We can, however, use arguments of self-consistency to place plausible lower and upper bounds on the mass of the Higgs particle in the minimal model. A lower bound is obtained by computing[20] the first quantum corrections to the classical potential (10). Requiring that $\langle \phi \rangle \neq 0$ be an absolute minimum of the one-loop potential yields the condition

$$M_H^2 \geq \frac{3 G_F \sqrt{2}}{16 \pi^2} (2 M_W^4 + M_Z^4 - 4 m_t^4) \ , \qquad (24)$$

neglecting the contributions of scalar loops, which gives the nontrivial constraint

$$M_H^2 \geq (7 \text{ GeV}/c^2)^2 \cdot \left[1 - \left(\frac{m_t}{79 \text{ GeV}/c^2} \right)^4 \right] , \tag{25}$$

so long as m_t is not too large. When m_t exceeds 79 GeV/c^2, the loop-induced coefficient of $(\phi^\dagger \phi)^2 \log(\phi^\dagger \phi)$ changes sign and the potential becomes unbounded from below for large arguments, so the vacuum is unstable. The resulting constraint on M_H has been re-examined recently[21]. For top-quark masses of (90, 100, 110, 120, 180) GeV/c^2, the lower bounds on the mass of the Higgs boson are (7.4, 20, 34, 50, 165) GeV/c^2.

Unitarity arguments[22] lead to a conditional upper bound on the Higgs boson mass[23]. It is straightforward to compute the amplitudes $\mathcal{M}$ for gauge boson scattering at high energies and to make a partial-wave decomposition according to

$$\mathcal{M}(s,t) = 16\pi \sum_{J=0}^{\infty} (2J+1) a_J(s) P_J(\cos\theta) . \tag{26}$$

Most channels "decouple," in the sense that partial-wave amplitudes are small at all energies (except very near the particle poles, or at exponentially large energies), for any value of the Higgs boson mass M_H. Four channels are interesting:

$$W_L W_L$$
$$Z_L Z_L / \sqrt{2}$$
$$HH / \sqrt{2}$$
$$H Z_L$$

where the subscript L denotes the longitudinal polarization states, and the factors of $\sqrt{2}$ account for identical particle statistics. For these, the s-wave amplitudes are all asymptotically constant (i.e., well-behaved) and proportional to $G_F M_H^2$. In the high-energy limit,

$$\lim_{s \gg M_H^2} (a_0) \rightarrow \frac{-G_F M_H^2}{4\pi\sqrt{2}} \cdot \begin{bmatrix} 1 & 1/\sqrt{8} & 1/\sqrt{8} & 0 \\ 1/\sqrt{8} & 3/4 & 1/4 & 0 \\ 1/\sqrt{8} & 1/4 & 3/4 & 0 \\ 0 & 0 & 0 & 1/2 \end{bmatrix} . \tag{27}$$

Requiring that the largest eigenvalue respect the partial-wave unitarity condition $|a_0| \le 1$ yields

$$M_H < \left(\frac{8\pi\sqrt{2}}{3G_F}\right)^{1/2} \simeq 1 \text{ TeV}/c^2 \tag{28}$$

as a condition for perturbative unitarity. If the bound is respected, weak interactions remain weak at all energies, and perturbation theory is everywhere reliable. If the bound is violated, perturbation theory breaks down, and weak interactions among $W^\pm$, Z, and H become strong on the 1-TeV scale. This means that the features of strong interactions at GeV energies will come to characterize electroweak gauge boson interactions at TeV energies. We interpret this to mean that new phenomena are to be found in the electroweak interactions at energies not much larger than 1 TeV.

Extensive analytic and numerical calculations of the standard model on the lattice suggest[24] that the cutoff parameter in the lattice regularization can be substantially greater than the Higgs-boson mass only if the mass does not significantly exceed 640 ± 40 GeV/c^2.

Phenomenological portraits of the Higgs boson have appeared regularly in recent years[25-29]. Here we recall a few basic characteristics that influence the search for the Higgs boson. The role of the Higgs boson in generating fermion masses means that decays into heavy fermion-antifermion pairs are favored. The partial width is given by

$$\Gamma(H \rightarrow f\bar{f}) = \frac{G_F M_H m_f^2}{4\pi\sqrt{2}} N_c , \tag{29}$$

where N_c is the dimension of the $SU(3)_c$ representation of the fermions.

As the Higgs-boson mass increases beyond twice the mass of the interme-diate boson, decays into pairs of gauge bosons rapidly become predominant, be-cause of the strong coupling between the Higgs boson and longitudinal compo-nents of gauge bosons that led to the constraint (28). The partial widths are

$$\Gamma(H \to W^+ W^-) = \frac{G_F M_H^3}{32\pi\sqrt{2}} (1 - x)^{1/2}(4 - 4x + 3x^2) \quad, \tag{30}$$

where $x = 4M_W^2/M_H^2$, and

$$\Gamma(H \to Z^0 Z^0) = \frac{G_F M_H^3}{64\pi\sqrt{2}} (1 - x')^{1/2}(4 - 4x' + 3x'^2) \quad, \tag{31}$$

where $x' = 4M_Z^2/M_H^2$. Far above threshold, the main decay products are longitudinally polarized gauge bosons. In the final factor of (30), for example, the contribution of helicities $+ +$ or $- -$ is x^2; the LL contribution is $4 - 4x + x^2$. The growth of these partial widths with Higgs-boson mass is shown in Figure 2 for a top-quark mass of 125 GeV/c^2. The proportionality $\Gamma_H \propto M_H^3$ means that the width of a 1-TeV/c^2 Higgs boson is about 500 GeV—hardly a narrow resonance.

Provided the event rates are adequate, the decay into a pair of neutral gauge bosons that subsequently decay into charged-lepton pairs is an inviting mode for the discovery of a heavy Higgs boson. In the intermediate mass regime, $M_W < M_H < 2M_W$, detection of the Higgs boson will be more challeng-ing. Branching fractions for some modes that may prove detectable are dis-played in Figure 3 for a top-quark mass of 125 GeV/c^2.

THE IMPORTANCE OF THE 1-TEV SCALE

To this point, we have outlined the standard electroweak theory and empha-sized that the need for a Higgs boson or substitute is quite general. We have also reviewed the properties of the standard-model Higgs boson. By consider-

ing a thought-experiment, the scattering of pairs of gauge bosons at very high energies, we found a first signal for the importance of the 1-TeV scale. How to carry out this thought-experiment in the laboratory is discussed at the end of my second lecture and, at much greater length, in the series of lectures by Mike Chanowitz. In this section, we shall see how another path also leads to the 1-TeV scale.

Although the standard model shows us how a consistent electroweak theory might be constructed, we know that it must be incomplete[1,30]. The standard model does not explain how the scale of electroweak symmetry breaking is maintained in the presence of quantum corrections[31]. Beyond the classical approximation, scalar mass parameters receive quantum corrections involving loops of particles of spins $J = 1, \frac{1}{2},$ and 0. The loop integrals that enter the expression for scalar masses,

$$m^2(p^2) = m^2(\Lambda^2) + Cg^2 \int_{p^2}^{\Lambda^2} dk^2 + .. \,, \qquad (32)$$

are potentially divergent. Here Λ defines a reference scale at which the value of m^2 is known, g is the coupling constant of the theory, and C is a constant of proportionality, calculable in any particular theory. For the mass shifts induced by radiative corrections to remain under control (i.e., not to greatly exceed the value measured on the laboratory scale), either (i) Λ must be small, so the range of integration is not enormous, or (ii) new physics must intervene to cut off the integral.

In the standard $SU(3)_c \otimes SU(2)_L \otimes U(1)_Y$ model, the natural reference scale for Λ is the Planck mass, $M_{\text{Planck}} \approx 10^{19}$ GeV. In a unified theory of the strong, weak, and electromagnetic interactions, the natural scale is the unification scale, $M_U \approx 10^{15}$ GeV. Both estimates are very large compared with the scale of electroweak symmetry breaking $v = \sqrt{-\mu^2/|\lambda|} = (G_F\sqrt{2})^{-1/2} \approx 246$ GeV. We are therefore assured that new physics must intervene at an energy of approximately 1 TeV, in order that mass shifts not be much larger than v.

What form might the new physics take? Supersymmetry exploits the fact that fermion loops contribute with an overall minus sign (because of Fermi

statistics) to balance the contributions of fermion and boson loops in (32). In the limit of unbroken supersymmetry, in which the masses of bosons are equal to the masses of their fermion counterparts, the cancellation is exact and the quadratic divergence is eliminated. If the supersymmetry is broken, the contribution of the loop integrals may still be acceptably small if the fermion-boson mass splittings are less than about 1 TeV/c^2.

A second solution to the broad range of integration in (32) is offered by theories in which the scalars—and perhaps the fermions and gauge bosons—are composite on the 1-TeV scale. Thus the effective range of interaction is cut off, and mass shifts are controlled. A third (and minimalist) possibility, which entails the sacrifice of perturbation theory for the electroweak interactions, is that of a strongly interacting gauge sector. This would give rise to WW resonances, multiple production of Higgs bosons, and other new phenomena.

Theory alone cannot decide which solution—if any of these—Nature has chosen. We can be certain that a thorough exploration of the 1-TeV scale will give us a detailed understanding of how the electroweak symmetry is broken. That sets the first goal of the next generation of accelerators.

HADRON SUPERCOLLIDERS

This second lecture considers how incisive physics can be done using multi-TeV hadron colliders. Let us begin by looking more closely at the two machines being planned.

The SSC site lies about 40 km south of Dallas. The collider tunnel, with a circumference of about 86 km, will contain two separate rings of superconducting magnets, separated vertically by about 80 cm. Initially, there will be two high-luminosity and two intermediate-luminosity interaction regions. The design includes the possibility of adding bypasses that would double the number of experimental areas. A sketch of the SSC layout is shown in Figure 4. The main parameters[32] are listed in Table II.

Table II   Principal parameters of the SSC.

Number of particles/bunch	$N =$	0.80×10^{10}
Number of bunches/ring		1.60×10^{4}
Filling factor	$F =$	92%
Bunch collision frequency	$f =$	60 MHz
Bunch separation		5.0 m
Average beam current / beam		71 mA
Bunch length (68% of bunch)	$2\sigma_z =$	12.0 cm
Amplitude function at IP	$\beta^* =$	$\begin{cases} 0.5 \text{ m at 2 IRs}^{\dagger} \\ 10.0 \text{ m at IRs}^{\dagger} \end{cases}$
Beam radius (68% of bunch)	$\sigma =$	$\begin{cases} 4.8\ \mu\text{m} \ (\beta^* = 0.5 \text{ m}) \\ 21.7\ \mu\text{m} \ (\beta^* = 10 \text{ m}) \end{cases}$
Crossing angle	$\alpha =$	0–150 μrad (adjustable)
Length of luminous region (68% of interactions)		$\begin{cases} \dfrac{12.0}{\sqrt{2+7.8 \times 10^7 \alpha^2}}\text{cm}\ (\beta^* = 0.5 \text{ m}) \\[2ex] \dfrac{12.0}{\sqrt{2+3.8 \times 10^6 \alpha^2}}\text{cm}\ (\beta^* = 10 \text{ m}) \end{cases}$
Crossing time (68% of interactions)		0.28 ns
Standard luminosity	$\mathscr{L} =$	$\begin{cases} 10^{33}\text{ cm}^{-2}\text{s}^{-1} \quad (\beta^*=0.5 \text{ m, } \alpha=75\ \mu\text{rad}) \\ 5.5\times10^{31}\text{ cm}^{-2}\text{s}^{-1} \ (\beta^*=10 \text{ m, } \alpha=75\ \mu\text{rad}) \end{cases}$
Mean interactions/crossing		$\begin{cases} 1.8 \quad (\beta^* = 0.5 \text{ m}) \\ 0.09 \quad (\beta^* = 10 \text{ m}) \end{cases}$
Power radiated from collisions		$\begin{cases} 580 \text{ J/s} \quad (\beta^* = 0.5 \text{ m}) \\ 30 \text{ J/s} \quad (\beta^* = 10 \text{ m}) \end{cases}$
Luminosity lifetime		~24 hr
Free space at IP		$\begin{cases} \pm 20 \text{ m} \quad (\beta^* = 0.5 \text{ m}) \\ \pm 120 \text{ m} \quad (\beta^* = 10 \text{ m}) \end{cases}$

†Low-β^* or high-β^* regions are paired together in series in the same diamond.

At CERN, a Large Hadron Collider is being considered for installation in the LEP tunnel. It would make use of very-high-field superconducting magnets arrayed side by side in a single cryostat. Three of the undeveloped LEP straight sections could be exploited for proton-proton collisions, as shown in Figure 5. Some of the characteristics of the current LHC design[33] are collected in Table III.

TABLE III   Principal parameters of the Large Hadron Collider at CERN.

Circumference	26658.833	m
Revolution time	88.924	μs
Revolution frequency	11.246	kHz
Nominal bending field	10.0	T
Nominal beam energies	8	TeV
Injection energy	0.45	TeV
Number of interaction regions		
high luminosity	1	
medium luminosity	2	
Free space for experiments		
high luminosity	$\pm$12	m
medium luminosity	$\pm$40	m
Full bunch length (4σ)	0.31	m
RF frequency	400.8	MHz
Acceleration time	1200	s
Interbunch spacing	15	ns
Proton bunches / beam	4810	
Protons / bunch	$1.0 \cdot 10^{11}$	
Protons / beam	$4.81 \cdot 10^{14}$	
Beam current	865	mA
Stored energy / beam	597	MJ
Total synchrotron radiation	18.3	kW
Beam radius (4σ) at β^*=0.25 m	21	μm
Design luminosity at β^*=0.25 m	$3 \cdot 10^{34}$	$cm^{-2}s^{-1}$

WHAT IS A PROTON?

For the construction of large accelerators, we are limited to beams of charged, stable particles, which means electrons and protons and their antiparticles. With current methods, it is feasible to produce intense proton beams of

tens of TeV, but electron beams of only about a tenth of a TeV. So far as we know, the electron is an elementary point particle ($r_e \lesssim 10^{-16}$ cm), but the proton is a composite system. Our ability to exploit the energy advantage of proton beams therefore depends on our knowledge of what a proton is, and how it behaves in high energy collisions. Let us look briefly at what we know about proton structure.

The static properties of a proton are well characterized by a description of a proton as a three-quark (uud) bound state, with a radius $r_p \approx 1$ fm. This picture accounts for the essential features of magnetic moments, axial charges, electromagnetic form factors, and such[34].

In a violent collision, a proton is a broad-band, unselected beam of quarks, antiquarks, and gluons—and possibly other constituents. The composition of this mixed beam depends on how you inspect it: the more virtual the probe, the more sensitive it will be to short time-scale fluctuations.

It is fruitful to analyze the proton in the framework of the parton model with QCD refinements. The fundamental quantity in this picture is $f_i^{(a)}(x_a, Q^2)$, the number density of partons of species i with momentum fraction x_a of hadron a seen by a probe with resolving power characterized by Q^2.

Up to now, the best information on parton distributions (or hadron structure functions) comes from measurements of deeply inelastic lepton scattering, the reactions

$$eN \rightarrow e + \text{anything} , \tag{33}$$

$$\mu N \rightarrow \mu + \text{anything} , \tag{34}$$

$$\nu_\mu N \rightarrow \mu + \text{anything} , \tag{35}$$

and

$$\nu_\mu N \rightarrow \nu_\mu + \text{anything} . \tag{36}$$

For the scattering of charged leptons from nucleons at present energies, the probe is a virtual photon (with usually negligible corrections for the exchange of a virtual Z^0). In the charged-current neutrino reaction, the nucleon is probed by $W^{\pm}$; in the neutral-current neutrino reaction, the probe is the Z^0.

The kinematic notation for deeply inelastic scattering is indicated in Figure 6. From the four-momenta indicated there we may form the useful invariants

$$s = (\ell + P)^2$$
$$Q^2 = -q^2 = -(\ell - \ell')^2 \tag{37}$$
$$v = q \cdot P/M$$

where M is the target mass and $W^2 = 2Mv + M^2 - Q^2$ is the square of the invariant mass of the produced hadronic system "anything." It is convenient to work in terms of Bjorken's dimensionless variables

$$x = Q^2/2Mv \ , \tag{38}$$

the momentum fraction of the struck parton, and

$$y = v/E_{lab} \ , \tag{39}$$

the fractional energy loss of the lepton in the laboratory frame.

For electromagnetic scattering, we may write the differential cross section as

$$\frac{d\sigma}{dxdy} = \frac{4\pi\alpha_s^2}{Q^4}\left[F_2(x)(1-y)+F_1(x)xy^2\right] \ . \tag{40}$$

In the parton model, $2xF_1(x) = F_2(x)$, and the structure function F_2 of the proton may be written as

$$F_2^{ep}(x)/x = \frac{4}{9}[u(x) + \overline{u}(x)] + \frac{1}{9}[d(x) + \overline{d}(x)] + \frac{1}{9}[s(x) + \overline{s}(x)] + ... \tag{41}$$

The structure function of the neutron is obtained by an isospin rotation, which is to say, by the replacement $u \leftrightarrow d$. The parton distributions satisfy the momentum sum rule,

$$\sum_{\substack{i \,=\, parton \\ species}} \int_0^1 dx \, x f_i(x) = 1 \ . \tag{42}$$

An important early result was the recognition that charged partons do not carry all the momentum of the nucleon. We may see this by approximating

$$F_2^{ep}(x) + F_2^{en}(x) = \frac{5x}{9} [u(x) + \bar{u}(x) + d(x) + \bar{d}(x)] \ . \tag{43}$$

A measurement of F_2 then leads to an estimate of the momentum carried by charged partons—specifically, up and down quarks and antiquarks—through the connection

$$\frac{9}{5} \int_0^1 dx [F_2^{ep}(x) + F_2^{en}(x)] = \sum_{\substack{i \,=\, quarks\, + \\ antiquarks}} \int_0^1 dx \, x f_i(x) \ . \tag{44}$$

The experimental value of the integral of F_2 is about 0.45, almost independent of Q^2. Unless most of the momentum of the nucleon is carried by strange (and heavier) quarks, this implies that about half the momentum of a proton is carried by neutrals.

Charged-current scattering of neutrinos from nucleons has also been studied extensively. We define an "isoscalar nucleon" $N = \frac{1}{2}(p + n)$. The differential cross sections for scattering of neutrinos and antineutrinos are then

$$\frac{d\sigma(\nu N \rightarrow \mu^- + X)}{dxdy} = \frac{G_F^2 ME}{\pi} \Big[(u(x) + d(x)) + (\bar{u}(x) + \bar{d}(x))(1-y)^2 \Big] \ , \tag{45}$$

$$\frac{d\sigma(\bar{\nu} N \rightarrow \mu^+ + X)}{dxdy} = \frac{G_F^2 ME}{\pi} \Big[(u(x) + d(x))(1-y)^2 + (\bar{u}(x) + \bar{d}(x)) \Big] \ . \tag{46}$$

The difference $\sigma(vN) - \sigma(\bar{v}N)$ allows a determination of the excess of quarks over antiquarks, i.e., the distribution of "valence" quarks that determine the nucleon quantum numbers:

$$u(x) - \bar{u}(x) + d(x) - \bar{d}(x) = u_{valence} + d_{valence} \qquad (47)$$

Viewed at very long wavelengths, the proton appears structureless, but as Q^2 increases and the resolution becomes finer, the proton is revealed as a composite object characterized, for example, by rapidly falling elastic form factors that decrease as $1/Q^4$. According to the parton model, which ignores interactions among the constituents of the proton, the picture for deeply inelastic scattering is then exceedingly simple. Once Q^2 has become large enough for the quark constituents to be resolved, no finer structure is seen. The quarks are structureless, have no size, and thus introduce no length scale. When Q^2 exceeds a few GeV^2, all fixed mass scales become irrelevant and the structure functions and parton distributions do not depend upon Q^2. This is approximately so in Nature, as may be seen from the compilation of measurements of $F_2^{\mu p}(x)$ shown in Figure 7.

In an interacting field theory, however, a more complex picture of hadron structure emerges. As Q^2 increases beyond the magnitude required to resolve quarks, the quarks themselves are found to have an apparent structure, which arises from the interactions mediated by the gluon fields. The parton distributions evolve with Q^2 as a result of quantum fluctuations shown there. The virtual dissociation of a quark into a quark and gluon degrades the valence quark distribution. The virtual dissociation of a gluon into a $q\bar{q}$ pair enhances the population of quarks and antiquarks.

It is therefore plausible to expect, in any interacting field theory, that as Q^2 increases the structure function will fall at large values of x and rise at small values of x. In most field theories, there is a power-law dependence on Q^2, but in asymptotically free gauge theories, such as QCD, the dependence on Q^2 is only logarithmic.

The evolution of neutrino structure functions is indicated in Figure 8, which shows the Q^2-dependence of

$$\mathcal{F}_2^{\nu N} = x\left[u(x) + \overline{u}(x) + d(x) + \overline{d}(x)\right] , \qquad (48)$$

and in Figure 9,which displays that of the flavor-nonsinglet structure function

$$x\mathcal{F}_3^{\nu N} = x\left[u(x) - \overline{u}(x) + d(x) - \overline{d}(x)\right] . \qquad (49)$$

The latter, which measures the valence quark distribution, is of special interest because it receives no contribution from the dissociation of gluons into quark-antiquark pairs; it is simply degraded, with increasing Q^2, by gluon radiation from the valence quarks. It therefore offers, in principle, a means for studying the evolution of the quark distributions uncomplicated by the need to know anything about the gluon distribution.

Once parton distributions have been measured in detail at some value of $Q^2 = Q_0^2$, and the running coupling constant $\alpha_s(Q^2)$ of the strong interactions has been determined, QCD permits us to compute the parton distributions at higher values of Q^2. A convenient formalism is provided by the Altarelli-Parisi equations[35], integro-differential equations for the parton distributions[36]. It is worth recalling a few of the essentials here.

It is conventional to parametrize the strong coupling constant as

$$1/\alpha_s(Q^2) = \frac{33-2N_f}{12\pi} \log(Q^2/\Lambda^2) , \qquad (50)$$

where N_f is the number of "active" quark flavors, and to determine Λ from the evolution of structure functions. For example, if we define the second moment

$$\Delta_2(Q^2) = \int_0^1 dx \, x \, [u_v(x)+d_v(x)] \qquad (51)$$

of the valence quark distribution, then the Altarelli-Parisi equations give

$$\frac{\Delta_2(Q^2)}{\Delta_2(Q_0^2)} = \left[\frac{\alpha_s(Q_0^2)}{\alpha_s(Q^2)}\right]^{6A_2/(33-2N_f)} \quad , \tag{52}$$

where $A_2 \approx -1.78$. Knowing $\int_0^1 dx \, x\mathcal{F}_3(x,Q^2)$ at different values of Q^2 thus allows, in principle, a direct determination of the QCD scale parameter Λ. In practice, the limited statistics of neutrino experiments, the small available range in $\log(Q^2)$, and other factors limit the precision of such determinations.

If the evolution of $F_2^{\mu N}$ or $\mathcal{F}_2^{\nu N}$, either of which is measured with higher statistics than $x\mathcal{F}_3^{\nu N}$, is to be used for a determination of Λ, we are faced with the problem that the gluon distribution is not measured directly in lepton scattering. Its character must be inferred from the rate of evolution of the antiquark distribution and so is coupled with the value of Λ. Finally, let us note that no detailed measurements have been carried out for values of $x \lesssim 10^{-2}$. This gap will be filled by experiments at the *ep* collider HERA.

The discovery reach of a hadron supercollider is determined by hard scattering processes in which the constituents interact at high energies, as depicted in Figure 10. Cross sections may be calculated in the renormalization group improved parton model, provided we know the behavior of the quark and gluon distributions within the proton as functions of x and Q^2. For the parton subprocesses of interest, the range over which the structure functions must be known is

$$(10 \text{ GeV})^2 \lesssim Q^2 \lesssim (10^4 \text{ GeV})^2 \, , \tag{53}$$

which may correspond to $<x>$ as small as 10^{-4}. With the parton distributions written as $f_i^{(a)}(x_a,Q^2)$ for the number density of partons of species i in hadron a, hadronic cross sections are given schematically by

$$d\sigma(a+b \to c+X) = \sum_{ij} \int dx_a dx_b \, f_i^{(a)}(x_a,Q^2) \, f_j^{(b)}(x_b,Q^2) \, d\hat{\sigma}(i+j \to c+X) \, , \tag{54}$$

where $d\hat{\sigma}$ represents the elementary cross section. The parton-level cross sections are known for a great many reactions of potential interest.

In EHLQ[1] we produced two sets of distribution functions that behave sensibly over the kinematic range of interest. This was done by constructing initial distributions at $Q_0^2 = 5$ GeV^2 using the CDHS structure functions[37], subject to the constraints of momentum and flavor sum rules, and under the assumption that there are no intrinsic heavy-flavor components. We then evolved the distributions to $Q^2 > Q_0^2$ using the (first-order) Altarelli-Parisi equations. We studied in detail two distributions, characterized by the QCD scale parameters $\Lambda = $ 200 MeV and 290 MeV, and considered the uncertainties at length. The two sets of input distributions are extracted assuming that $\sigma_L/\sigma_T \approx 0.1$ (Set 1), or that the ratio σ_L/σ_T is as given by QCD (Set 2). At $Q_0^2 = 5$ GeV^2, these are characterized by

$$xu_v(x,Q_0^2) = 1.78\ x^{0.5}(1-x^{1.51})^{3.5}$$

$$xd_v(x,Q_0^2) = 0.67\ x^{0.4}(1-x^{1.51})^{4.5}$$

$$xu_s(x,Q_0^2) = 0.182\ (1-x)^{8.54}$$

$$xs_s(x,Q_0^2) = 0.081\ (1-x)^{8.54}$$

$$xG(x,Q_0^2) = (2.62+9.17x)(1-x)^{5.90}$$

$$\Lambda = 200\ \text{MeV}$$

(55)

for Set 1, and

$$xu_s(x,Q_0^2) = 0.185\ (1-x)^{7.12}$$

$$xs_s(x,Q_0^2) = 0.0795\ (1-x)^{7.12}$$

$$xG(x,Q_0^2) = (1.75+15.575x)(1-x)^{6.03}$$

$$\Lambda = 290\ \text{MeV}$$

(56)

with the same valence distributions for Set 2. A rather complete discussion of the properties of the resulting distributions is given in EHLQ.

As a final partial answer to our question, "What is a proton?" let us look at the flavor content of the proton, as measured by the momentum fraction

$$\int_0^1 dx \; x f_i(x,Q^2) \tag{57}$$

carried by each parton species. This is shown in Figure 11 for the EHLQ 1986 Set 2. As Q^2 increases, momentum is shared more and more equally among the quark and antiquark flavors, reflecting the trend toward the asymptotic values

$$\int_0^1 dx \; x G(x,Q^2 \to \infty) = \frac{8}{17}$$

$$\int_0^1 dx \; x q_s(x,Q^2 \to \infty) = \frac{3}{68} \quad \text{(each flavor)} \tag{58}$$

$$\int_0^1 dx \; x q_v(x,Q^2 \to \infty) = 0$$

expected in QCD with six quark flavors and no light colored superpartners. It is easy to verify that the momentum sum rule (42) is satisfied:

$$\frac{8}{17} \text{ (gluons) } + 6 \text{ flavors} \cdot 2 \text{ (quarks+antiquarks)} \cdot \frac{3}{68} = 1. \tag{59}$$

The EHLQ structure functions were evolved assuming a top-quark mass that then seemed reasonable, $m_t = 35$ GeV/c^2. The population of top quarks would be even smaller if the current lower bound, $m_t > 89$ GeV/c^2, were used.

The current state of our knowledge—both experimental and theoretical—of structure functions was assessed recently in a workshop at Fermilab[38].

PARTON-PARTON LUMINOSITIES

Given a proton-proton collision at energy $\sqrt{s}$, what is the luminosity of parton-parton collisions at a lower energy $\sqrt{\hat{s}}$? One convenient measure of the rate of parton-parton collisions is the differential luminosity

$$\tau \frac{d\mathcal{L}}{d\tau} = \frac{\tau}{1 + \delta_{ij}} \int_{\tau}^{1} dx \left[f_i^{(a)}(x, Q^2) f_j^{(b)}(\tau/x, Q^2) + f_j^{(a)}(x, Q^2) f_i^{(b)}(\tau/x, Q^2) \right] / x , \quad (60)$$

where $f_i^{(a)}(x, Q^2)$ is the number distribution of partons of species i carrying momentum fraction x of hadron a. The scaling variable τ is given by

$$\tau = \hat{s} / s . \tag{61}$$

The differential luminosity represents the number of parton-parton collisions with scaled c.m. energies in the interval $(\tau, \tau + d\tau)$ per hadron-hadron collision. Thus the differential cross section for the hadronic reaction

$$a + b \rightarrow \alpha + \text{anything} \tag{62}$$

is given by

$$\frac{d\sigma}{d\tau}(ab \rightarrow \alpha X) = \sum_{ij} \frac{d\mathcal{L}}{d\tau} \hat{\sigma}(ij \rightarrow \alpha) , \tag{63}$$

where $\hat{\sigma}(ij \rightarrow \alpha)$ is the cross section for the operative elementary process.

The interesting hard-scattering processes that define much of the physics motivation of a multi-TeV collider have a common asymptotic form prescribed by dimensional analysis,

$$\hat{\sigma}(\hat{s}) = K/\hat{s} . \tag{64}$$

For a typical electroweak reaction, $K \sim (\alpha/\pi)^2$, while for a typical strong-interaction process, $K \sim (\alpha_s/\pi)^2$. Resonance production cross sections are proportional to τ. Consequently, the quantity $(\tau/\hat{s})\frac{d\mathcal{L}}{d\tau}$, which has dimensions of a cross section, provides a useful measure of the reach of a collider of given energy and hadron-hadron luminosity. I show in Figures 12–15 the effective luminosities for gg, uu, $u\bar{u}$, and $d\bar{d}$ collisions, for proton-proton collisions at $\sqrt{s} = $ 10, 17, 20, 30, 35, and 40 TeV.

Valence quarks in high-energy protons act as copious sources of quasireal gauge bosons, in much the same fashion as high-energy electron beams act as copious sources of quasireal photons. The recognition[39-44] that the luminosity for gauge-boson interactions in multi-TeV proton-proton collisions is appreciable has made it possible to contemplate carrying out in practice the thought-experiment discussed in the first lecture and has significantly extended the search for a heavy Higgs boson. The luminosities for scattering of longitudinally polarized W and Z are displayed in Figures 16 and 17.

THE EXPERIMENTAL ENVIRONMENT AT SUPERCOLLIDERS

Signals and backgrounds for specific phenomena at multi-TeV hadron colliders have been studied extensively[1-13]. To design experiments, it is also important to be aware of the general environment in which detectors must function and events must be selected and recorded. At the SSC's design luminosity of 10^{33} cm^{-2}s^{-1}, we expect about 10^8 inelastic collisions per second and an average of 1.7 events per crossing. Interaction rates at the LHC may be considerably higher. A general-purpose detector[45-47] will have about 10^6 electronic channels.

A good way to gain respect for the conditions that will prevail at the SSC is to examine the trigger rate for events containing single jets with transverse momentum $p_\perp$ exceeding some threshold p^{min}. This is shown in Figure 18 for the nominal operating conditions of the SSC: $\sqrt{s}$ = 40 TeV and $\mathscr{L}$ = 10^{33} cm^{-2} s^{-1}. At 40 TeV, a high-$p_\perp$ trigger with threshold set at $p_\perp$ > 0.9 TeV/c in the rapidity interval $|y|$ < 4 will count at 1 Hz from QCD jets. This is of interest in planning efficient triggers to select interesting events.

Tracking is indispensable for distinguishing an isolated electron from the other particles—photons—that initiate electromagnetic showers. At large transverse momentum, the overwhelming number of electromagnetic showers will come from photons. I show in Figure 19 the cross section for the production in 40-TeV pp collisions of an isolated positron with transverse momentum $p_\perp$ > p^{min}, for several cuts in rapidity. Isolated means that the particle is

accompanied by less than 10 GeV of hadronic energy in a cone of radius $\Delta R =$ $\sqrt{\Delta \eta^2 + \Delta \phi^2}$ = 0.7 about its direction. Except at the lowest values of transverse energy, where semileptonic decays of c and b quarks contribute appreciably, the chief source of isolated positrons is from leptonic decays of W^+ and Z^0, which may be produced in association with hadron jets. The matching plot in Figure 20 shows the corresponding cross sections for the production of prompt photons. At $\mathscr{L} = 10^{33}$ cm^{-2} sec^{-1} a threshold of $E_T > 450$ GeV in the rapidity interval $|y| < 4$ for isolated photons selects one event a minute. One event per second is recorded with a threshold of about 140 GeV. The ratio of prompt photons to positrons is nowhere less than an order of magnitude. This means that, without tracking information or other particle identification, almost every large-$p_\perp$ electron found by calorimetry is really a photon.

SOME DISCOVERY POSSIBILITIES FOR HADRON COLLIDERS

In this final lecture, I wish to survey the range of experimental targets for multi-TeV colliders. The parameters of the SSC and the LHC have been set by considering the demands of hard-scattering processes and by our conviction that it is essential for the next machine to make possible a thorough exploration of the 1-TeV scale. This has been a sensible way to proceed, because the scientific goals are of high importance and because these are the reactions that make the most severe demands on energy and luminosity (both instantaneous and average), the parameters that drive accelerator design. However, the experimental program of a multi-TeV collider will be broader than the set of experiments we use to define the capabilities of the machine. It is very important that our vision of experiments or of detector components not be narrowed by what QCD predicts or what theorists find most interesting today. Similarly, we must not assume that every experiment will take the form of a general-purpose device with full angular coverage.

An initial program of exploration might well include measurements expected to be prosaic, but with the capacity to surprise, such as particle surveys of the kind carried out in the past with highly instrumented single-arm spec-

trometers. Though a pp collider does not seem to be the most favorable environment for producing a quark-gluon plasma, it would be a mistake to deny ourselves the opportunity to look for signs of changes of phase: copious production of strange particles, or of photons, as well as changes in the kinematical characteristics of events. Similar remarks apply to every kind of "zoo" event hinted in cosmic-ray experiments.

In what follows, I shall give examples of the discovery reach of the SSC operating at 40 TeV and 10^{33} cm^{-2}s^{-1}. I am confident (from my own studies and from the work of others designing detectors) that these estimates are reasonable, and likely to be realized or surpassed. I am less certain about the range of measurements for which the LHC's peak luminosity can be utilized. This question is under intensive study by an ECFA working group and should be far better understood before the end of 1990.

Precision measurements from CDF

Physics advances both by the search for new phenomena and by the detailed study of familiar observables. The great variety of precise measurements to be expected from a multipurpose detector operating at a hadron collider is evident in new results obtained by the CDF collaboration at the Tevatron. Since these observations are treated in greater detail in the lectures by John Peoples[49], I shall mention them only briefly here.

CDF's precision measurement of the mass and width of the Z^0 boson[50] was supported by high-resolution studies of the ψ and T states that have recently made possible the reconstruction of $\chi_c \rightarrow \gamma \psi (\rightarrow \mu^+ \mu^-)$. Very promising for the future of high-statistics B studies in hadron colliders is the identification of about a dozen examples of $B^\pm \rightarrow K^\pm \psi$ in the sample of $\psi \rightarrow \mu^+ \mu^-$ from the 1988–1989 CDF run[51]. The next run will incorporate a silicon vertex detector and special triggers to enrich the sample of B-mesons logged.

Compositeness

In a hadronic collision, useful kinematic variables are $p_\perp$, the transverse momentum of either jet, and the jet rapidities

$$y = \frac{1}{2} \log \left(\frac{E+p_z}{E-p_z} \right) ,$$

(65)

where p_z is the component of jet momentum along the beam. The dominant characteristic of many of these reactions is an angular dependence

$$\frac{d\sigma}{d\cos\theta} \sim \frac{1}{(1-\cos\theta)^2} ,$$

(66)

arising from the t-channel gluon exchange, analogous to the t-channel photon exchange that drives the Rutherford formula. In terms of the variable $\chi \equiv \cot^2(\theta/2)$, the angular distribution may be re-expressed as

$$\frac{d\sigma}{d\chi} \sim \text{constant} .$$

(67)

The angular distribution of two-jet events in the dijet c.m. frame, for dijets with effective masses M(jet-jet) > 200 GeV/c^2 has been measured by the CDF collaboration[52]. To first approximation, the distribution is flat in χ, as our simple analogy with Rutherford scattering would suggest. In more detail, it agrees very precisely with the prediction of the parton model. This is representative of the degree to which the expectations of QCD are being checked in collider experiments.

Once we can trust in the predictions of QCD in detail, it becomes increasingly interesting to search for deviations from the standard model. The idea that the quarks and leptons are structureless, indivisible elementary particles is basic to our current understanding. Testing the elementarity of quarks and leptons is therefore high on the agenda for future experiments. If the quarks are composite, they can interact not only by exchanging gluons, but also through the interchange of their constituents. As Eichten, Lane, and Peskin have pointed out[53], for (anti)quark-(anti)quark collisions at energies approaching the compositeness scale Λ^*, the effect of this new reaction mechanism is to introduce a contact term of geometrical size into the scattering amplitude.

I show in Figure 21 the differential cross section $d\sigma/dp_\perp dy|_{y=0}$ for the reaction

$$p\,p \rightarrow \text{jet} + \text{anything} \qquad\qquad (69)$$

at 40 TeV, for elementary quarks ($\Lambda^* = \infty$) and for quarks composite on scales of 10, 15, and 20 TeV. The gross features of these curves are easily understood. Because the contact term modifies the cross section for (anti)quark-(anti)quark scattering, its effects are most apparent at the large values of $p_\perp$ for which valence quark interactions dominate the cross section. At 40 TeV and an integrated luminosity of 10^{40} cm^{-2}, SSC experiments will be able to probe scales of 15–20 TeV. Detailed measurements of the jet-jet angular distribution should extend the range of sensitivity. The first run of the CDF experiment at the Fermilab Tevatron, at an energy of $\sqrt{s} = 1.8$ TeV, has set a lower limit of about 0.7 TeV on the scale of quark compositeness[54].

New Forces

In the past, we have become aware of forces by observing their effects and have only later discovered the force-carriers. Experiments with multi-TeV colliders may produce new gauge bosons before we have detected their low-energy effects.

There are many reasons to be open to the possibility of new gauge bosons. A right-handed W-boson arises in a left-right symmetric electroweak gauge theory, based on the symmetry group $SU(2)_L \otimes SU(2)_R \otimes U(1)_Y$, that would restore parity invariance at high energy. Unification groups larger than $SU(5)$ contain extra $U(1)$ gauge symmetries, implying additional Z^0s. Specific examples are provided by the low-energy gauge groups emerging from superstring models. In a specific theory, the calculation of $W^\pm$ and Z^0 production rates is easily modified to yield an estimate of the cross section for the production of new gauge bosons. As an example, I show in Figure 22 the cross section for the production of a new W-boson with standard gauge couplings to the light quarks. For the 40-TeV energy projected for the SSC, we may anticipate sensitive searches out to a mass of about 6 TeV/c^2.

The exceptional group E_6 has a long history as a candidate group for the unification of the strong, weak, and electromagnetic interactions. Historically,

the motivation for considering E_6 derived mainly from the observation that it is the unifying group beyond $SO(10)$, which is in turn the unifying group beyond $SU(5)$:

$$E_6 \supset SO(10) \supset SU(5) \,. \tag{70}$$

The revival of interest in E_6 in recent years is owed to the possibility that it may be the surviving symmetry of the $E_8 \otimes E_8'$ internal symmetry group of the heterotic string[55]. Like all applications of superstring ideas to phenomenology, the "derivation" of E_6 is very vague and tentative. Nevertheless, it provides us with a reason to look again at some possible consequences of an E_6 gauge symmetry.

The spectrum of quarks and leptons can be read off from the fundamental 27 representation of the group:

E_6:	**27**	=		**16**		$\oplus$		**10**		$\oplus$	**1**	: $SO(10)$
	$SU(5)$:	**10**	$\oplus$	**5***	$\oplus$	**1**		**5**	$\oplus$	**5***	**1**	
		u		d^c		N_e^c		h		h^c	n	
		d		e				E^+		E^-		
		u^c		ν_e				N_E^c		ν_E		
		e^c										
charge $Q^{(\eta)}$		$-\frac{2}{3}$		$\frac{1}{3}$		$-\frac{5}{3}$		$\frac{4}{3}$		$\frac{1}{3}$	$-\frac{5}{3}$	

The $\mathbf{10} \oplus \mathbf{5^*}$ of $SU(5)$ constitute the standard generation. The remaining member of the **16** of $SO(10)$ is a right-handed neutrino. Among the novel particles characteristic of E_6, the new charge $-\frac{1}{3}$ weak isoscalar quark is of especial interest.

With respect to interactions, we are interested in a scheme for spontaneous symmetry breaking that will lead eventually to the low-energy symmetry $SU(3)_c \otimes SU(2)_L \otimes U(1)_Y$. Thus we wish to break

$$E_6 \rightarrow \cdots \rightarrow SU(3)_c \otimes SU(2)_L \otimes U(1)_Y [\otimes \mathcal{G}] \,, \tag{71}$$

where $\mathcal{G}$ denotes possible additional symmetries that survive to low energies. There are examples in superstring theories of symmetry breaking induced by an E_6 adjoint 78 of Higgs bosons. This leads naturally to one or more extra $U(1)$ factors at low energies, which in turn implies an extra gauge boson, Z', coupled to a new conserved current corresponding to the charge $Q^{(\eta)}$.

The Z' is somewhat harder to produce in $p^{\pm}p$ collisions than a standard Z^0 of the same mass, because the couplings to light quarks are inhibited. The branching ratio for the decay into charged leptons, for example, is

$$\Gamma(Z' \rightarrow e^+ e^-) \approx 3\%/n_g \ , \tag{72}$$

wh $_?$ is the number of generations, which is somewhat smaller (by about $1/r$ n that of the conventional Z^0. The production cross sections for the new Z' a   wn in Figure 23. We expect to be sensitive to this new object in the leptoi   ir channel for masses as large as about 3–4 TeV/c^2 at the SSC. If the couplings of the Z' are the same as those of the standard Z^0, the reach of the SSC is extended by about 1 TeV/c^2.

With less specific motivation, we may consider enlarging the gauge group of the strong interactions. Suppose that at high energies color is chiral[56], so that the gauge group becomes

$$\mathcal{G} = [SU(3)_L \otimes SU(3)_R]_c \otimes SU(2)_L \otimes U(1)_Y \ . \tag{73}$$

The ch   l-color symmetry may be broken at a scale above that of electroweak symm   breaking, leading to the gauge group of the standard model as we know it,

$$\mathcal{G} \rightarrow SU(3)_c \otimes SU(2)_L \otimes U(1)_Y \ , \tag{74}$$

or it may be broken at the electroweak scale, leading directly to the observed low-energy symmetry,

$$\mathcal{G} \rightarrow SU(3)_c \otimes U(1)_{em} \ . \tag{75}$$

The breakdown of chiral-color symmetry would give rise to a color octet of massive axial gluons, called axigluons (A). If the breaking occurred on the electroweak scale, we would expect the axigluon mass to be $M_A \approx 100\,\text{GeV}/c^2$, a possibility that we shall see is already ruled out. If the chiral color is broken above the Fermi scale, there is no prediction for the axigluon mass.

The axigluon decays into a pair of colored fermions, with a total width

$$\Gamma(A) = N\alpha_s^2(M_A^2)M_A/6 \quad , \tag{76}$$

where N counts the number of fermion species, in quark equivalents. The $Aq\bar{q}$ vertex that drives the decay is also responsible for the most important mechanism for axigluon production in pp collisions at high energies. The elementary reaction

$$q\bar{q} \to A \to q\bar{q} \quad , \tag{77}$$

corresponding to the formation of a massive strong-interaction resonance, significantly enhances the production rate of high–transverse-momentum jets over what would be produced by ordinary QCD processes[57].

At $\sqrt{s} = 40\,\text{TeV}$ and $\mathcal{L} = 10^{33}\text{cm}^{-2}\text{s}^{-1}$, an axigluon could be detected[58] for masses as large as 9 TeV/c^2, either in the transverse-momentum spectrum of jets, shown in Figure 24, or in the two-jet invariant-mass distribution, shown in Figure 25. Like the signals for quark compositeness, to which they bear some resemblance, the signals for axigluon formation are large and allow the exploration of high mass scales. The UA1 collaboration[59] has excluded axigluons in the mass interval $150\,\text{GeV}/c^2 < M_A < 310\,\text{GeV}/c^2$, and the current CDF exposure should provide sensitivity out to $M_A \approx 600\,\text{GeV}/c^2$.

New colored fermions

Heavy quarks are produced in the reactions $gg \to Q\bar{Q}$ and $q\bar{q} \to Q\bar{Q}$ and through the decays of $W^{\pm}$ and Z^0. The gauge-boson mechanism has the advantage of known cross sections—which is to say cross sections that can be measured from the leptonic decays of the gauge bosons—and calculable branching ratios.

However, they lead to very large rates only for the decays of real (not virtual) gauge bosons. This made them an attractive option for early searches for the top quark at the $S\bar{p}pS$ and at the Tevatron.

The cross sections for the strong interaction processes are known in QCD perturbation theory[60]: Under most circumstances, the process $gg \to Q\bar{Q}$ is dominant, and the reaction $q\bar{q} \to Q\bar{Q}$ makes a negligible contribution. I show in Figure 26 the yield of heavy quarks from these sources at the SSC. There we expect an event rate sufficient for the discovery of heavy quarks with masses up to about 2 TeV/c^2. An evaluation of the requirements for detection depends upon the decay chain. If the dominant decay of the next heavy quark is

$$Q \to t + W^- , \tag{78}$$

as it is likely to be, the ultimate decay products will be different if the top-quark mass is greater or less than the mass of the intermediate boson. We have already remarked that if the top quark has standard decays, its mass exceeds that of the W-boson, so we expect the chain $Q \to b + W^+ + W^-$. If the top quark has eluded detection below the W-mass because it has nonstandard decays, such as $t \to b + H^+$, the topology of the $Q\bar{Q}$ final state will depend on the decays of the charged Higgs boson.

Pairs of Electroweak Gauge Bosons

Incisive tests of the structure of the electroweak interactions may be achieved in detailed measurements of the cross sections for the production of W^+W^-, $W^\pm Z^0$, $Z^0 Z^0$, $W^\pm \gamma$, and $Z^0 \gamma$ pairs. The rate for $W^\pm \gamma$ production is sensitive to the magnetic moment of the intermediate boson. In the standard model there are important cancellations in the amplitudes for W^+W^- and $W^\pm Z^0$ production that rely on the gauge structure of the WWZ trilinear coupling. The $Z^0 Z^0$ and $Z^0 \gamma$ reactions do not probe trilinear gauge couplings in the standard model, but they are sensitive to nonstandard interactions such as might arise if the gauge bosons were composite. In addition, the W^+W^- and $Z^0 Z^0$ final states may be significant backgrounds to the detection of heavy Higgs bosons and possible new degrees of freedom.

The intrinsic interest in the process $q_i \bar{q}_i \to W^+ W^-$, which accounts in part
for plans to study $e^+ e^-$ annihilations at c.m. energies around 180 GeV at LEP,
arises from the sensitivity of the cross section to the interplay among the γ-,
Z^0-, and quark-exchange contributions. In the absence of the Z^0-exchange term,
the cross section for production of a pair of longitudinally polarized interme-
diate bosons is proportional to E_{cm}^2, in gross violation of unitarity. It is impor-
tant to verify that the amplitude is damped as expected. The mass spectrum of
$W^+ W^-$ pairs is of interest both for the verification of gauge cancellations and
for the assessment of backgrounds to heavy Higgs boson decays. This is shown
for intermediate bosons satisfying $|y| < 2.5$ in Figure 27. The number of pairs
produced at high energies may be adequate for a test of the gauge cancellations,
provided that the intermediate bosons can be detected with high efficiency.

The pairs of gauge bosons produced in WW, WZ, and ZZ scattering and
the search for a strongly interacting gauge sector are discussed in detail by Mike
Chanowitz in his lectures.

The Higgs Boson

A heavy Higgs boson (by which we mean one with $M_H > 2M_Z$) will have the
characteristic signature of decay into a pair of gauge bosons, with branching
fraction roughly 2/3 into the $W^+ W^-$ channel and 1/3 into the $Z^0 Z^0$ channel.
Event rate permitting, the simplest mode in which to detect a heavy Higgs bo-
son is the four-charged-lepton final state arising from the decay chain

$$H^0 \to Z^0 \qquad Z^0$$
$$ \hookrightarrow \ell^+ \ell^- \quad \hookrightarrow \ell^+ \ell^- \quad . \tag{79}$$

The most promising mechanisms for Higgs-boson production are the gluon
fusion process and the intermediate-boson fusion process. The rate for gluon fu-
sion is sensitive to the masses of the quarks circulating in the loop, particularly
to the top-quark mass. I show in Figure 28 for various Higgs-boson masses the
yield of $Z^0 Z^0$ events detected through the cascade (79) in the reaction
$pp \to H^0$ + anything. The signal becomes less distinct at high masses, both be-
cause the number of events decreases and because the Higgs-boson width is pro-

portional to $G_F M_H^3$. The SSC should nevertheless allow us to carry out a thorough search for a heavy Higgs boson for masses approaching 1 TeV/c^2.

Technicolor

The dynamical symmetry-breaking approach, exemplified by technicolor theories, is modeled upon our understanding of another manifestation of spontaneous symmetry breaking in nature: the superconducting phase transition. The macroscopic order parameter of the Ginzburg-Landau phenomenology[62] corresponds to the wave function of superconducting charge carriers. It acquires a nonzero vacuum expectation value in the superconducting state. The microscopic Bardeen-Cooper-Schrieffer theory[63] identifies the dynamical origin of the order parameter with the formation of collective states of elementary fermions, the Cooper pairs of electrons. The basic idea of the technicolor mechanism is to replace the elementary Higgs boson of the standard model by a fermion-antifermion bound state. By analogy with the superconducting phase transition, the dynamics of the fundamental technicolor gauge interactions among technifermions generate scalar bound states, and these composite scalars play the role of the Higgs fields of the standard model.

In the case of superconductivity, the elementary fermions (electrons) and the gauge interactions (QED) needed to generate the scalar bound states are already present in the theory. Could we achieve a scheme of similar economy for the electroweak symmetry-breaking transition?

Consider an $SU(3)_c \otimes SU(2)_L \otimes U(1)_Y$ theory of massless up and down quarks. Because the strong interaction is strong, and the electroweak interaction is feeble, we may consider the $SU(2)_L \otimes U(1)_Y$ interaction as a perturbation. QCD has an exact (global) $SU(2)_L \otimes SU(2)_R$ chiral symmetry when the quarks are massless. At an energy scale $\sim \Lambda_{QCD}$, the strong interactions become strong, fermion condensates appear, and the chiral symmetry is spontaneously broken

$$SU(2)_L \otimes SU(2)_R \rightarrow SU(2)_V \qquad (79)$$

to the familiar strong-interaction flavor symmetry, isospin. Three Goldstone bosons appear, one for each broken generator of the original chiral invariance. These were identified by Nambu[64] as three massless pions.

The broken generators are three axial currents whose couplings to pions are measured by the pion decay constant f_π. When we turn on the $SU(2)_L \otimes U(1)_Y$ electroweak interaction, the electroweak gauge bosons couple to the axial currents and acquire masses of order $\sim gf_\pi$. The massless pions thus disappear from the physical spectrum, having become the longitudinal components of the weak gauge bosons. This achieves much of what we desire. Unfortunately, the mass acquired by the intermediate bosons is far smaller than required for a successful low-energy phenomenology; it is only[65]

$$M_W \sim 30 \text{ MeV}/c^2 \ . \tag{80}$$

The simplest transcription of these ideas to the electroweak sector is the minimal technicolor model of Weinberg[66] and Susskind[67]. The technicolor gauge group is taken to be $SU(N)_{TC}$ (usually $SU(4)_{TC}$), so the gauge interactions of the theory are generated by

$$SU(4)_{TC} \otimes SU(3)_c \otimes SU(2)_L \otimes U(1)_Y \ . \tag{81}$$

The technifermions are a chiral doublet of massless color singlets

$$\begin{pmatrix} U \\ D \end{pmatrix}_L \qquad U_R \qquad D_R \quad . \tag{82}$$

With the electric charge assignments $Q(U) = \frac{1}{2}$ and $Q(D) = -\frac{1}{2}$, the theory is free of electroweak anomalies. The ordinary fermions are all technicolor singlets.

In analogy with our discussion of chiral symmetry breaking in QCD, we assume that the chiral TC symmetry is broken,

$$SU(2)_L \otimes SU(2)_R \otimes U(1)_V \rightarrow SU(2)_V \otimes U(1)_V \ . \tag{83}$$

Three would-be Goldstone bosons emerge. These are the technipions

$$\pi_T^+ \qquad \pi_T^0 \qquad \pi_T^- \quad , \tag{84}$$

for which we are free to *choose* the technipion decay constant as

$$F_\pi = \left(G_F\sqrt{2}\right)^{-1/2} = 247\,\mathrm{GeV} \ . \tag{85}$$

When the electroweak interactions are turned on, the technipions become the longitudinal components of the intermediate bosons, which acquire masses

$$
\begin{aligned}
M_W^2 &= g^2 F_\pi^2 &= \pi\alpha/G_F\sqrt{2}\,\sin^2\theta_W \\
M_Z^2 &= (g^2 + g'^2)F_\pi^2 &= M_W^2/\cos^2\theta_W
\end{aligned}
\tag{86}
$$

that have the canonical standard model values, thanks to our choice (85) of the technipion decay constant.

Working by analogy with QCD, we may guess the spectrum of other $F\bar{F}$ bound states as follows:

$$
\left.
\begin{array}{lll}
1^{--} \text{ technirhos} & \rho_T^+ \ \rho_T^0 \ \rho_T^- \\
1^{--} \text{ techniomega} & \omega_T \\
0^{-+} \text{ technieta} & \eta_T \\
0^{++} \text{ technisigma} & \sigma_T
\end{array}
\right\} \quad ,
\tag{87}
$$

all with masses on the order of the technicolor scale $\Lambda_{TC} \sim O(1\,\mathrm{GeV}/c^2)$, since they do not originate as Goldstone bosons. The dominant decay of the technirho will be

$$\rho_T \to \pi_T\,\pi_T \ , \tag{88}$$

i.e., into pairs of longitudinally polarized gauge bosons. Standard estimates lead to

$$M(\rho_T) \approx 1.77 \text{ TeV}/c^2$$

$$(89)$$

$$\Gamma(\rho_T) \approx 325 \text{ GeV}$$

Technicolor shows how the generation of intermediate boson masses could arise without fundamental scalars or unnatural adjustments of parameters. It thus provides an elegant solution to the naturalness problem of the standard model. However, it has a major deficiency: it offers no explanation for the origin of quark and lepton masses, because no Yukawa couplings are generated between Higgs fields and quarks or leptons.

A possible approach to the problem of quark and lepton masses is suggested by "extended technicolor" models. We imagine that the technicolor gauge group is embedded in a larger extended technicolor gauge group,

$$G_{TC} \subset G_{ETC} ,$$

$$(90)$$

which couples quarks and leptons to the technifermions. If the ETC symmetry is spontaneously broken down to the TC symmetry

$$G_{ETC} \rightarrow G_{TC} ,$$

$$(91)$$

at a scale

$$\Lambda_{ETC} \sim 30 - 300 \text{ TeV} ,$$

$$(92)$$

then the quarks and leptons may acquire masses

$$m \sim \Lambda_{TC}^3 / \Lambda_{ETC}^2 .$$

$$(93)$$

The outlines of this strategy are given in References 68 and 69, but no "standard" ETC model has been constructed.

As a representative of the ETC strategy we may consider a model due to Farhi and Susskind[70]. Their model is built on new fundamental constituents, the techniquarks

$$\begin{pmatrix} U \\ D \end{pmatrix}_L \qquad U_R \qquad D_R \quad , \tag{94}$$

which are analogs of the ordinary quarks, and the technileptons

$$\begin{pmatrix} N \\ E \end{pmatrix}_L \qquad N_R \qquad E_R \quad , \tag{95}$$

which are analogs of the ordinary leptons. These technifermions are bound by the $SU(N)_{TC}$ gauge interaction, which is assumed to become strong at $\Lambda_{TC} \sim$ 1 TeV. Among the $F\bar{F}$ bound states are eight color-singlet, technicolor-singlet pseudoscalar states [labeled by (I, I_3)],

$$
\left.
\begin{aligned}
\pi_T^+ & \quad (1,1) \\
\pi_T^0 & \quad (1,0) \\
\pi_T^- & \quad (1,-1)
\end{aligned}
\right\} \quad \text{become longitudinal } W^\pm \text{ and } Z^0
$$

$$
\left.
\begin{aligned}
P^+ & \quad (1,1) \\
P^0 & \quad (1,0) \\
P^- & \quad (1,-1) \\
P^{0'} & \quad (0,0)
\end{aligned}
\right\} \quad \text{pseudo-Goldstone bosons} \tag{96}
$$

$$\eta_T' \quad (0,0) \qquad \text{techniflavor singlet}$$

plus the corresponding technivector mesons. Like the η' of QCD, the η_T' couples to an anomalous current, so it is expected to acquire a mass on the order of several hundred GeV/c^2. The pseudo-Goldstone bosons are massless in the absence of electroweak and ETC interactions.

We may combine the color triplet $(U\ D)$ and color-singlet $(N\ E)$ technifermions to build $^1S_0$ $(F\bar{F})$ states with masses (acquired from the color interaction) of

$$
\begin{aligned}
M(P_3) &\approx 160\,\text{GeV}/c^2 \\
M(P_8) &\approx 240\,\text{GeV}/c^2 \quad .
\end{aligned}
\tag{97}
$$

These include an isospin triplet P_3^1, P_3^0, P_3^{-1} of color triplets, an isospin singlet, color triplet state P_3', the corresponding antitriplet states, an isospin triplet P_8^+, P_8^0, P_8^- of color octets, and an isoscalar color-octet state $P_8^{0'}$. With standard charge assignments for the technifermions, the P_3 and P_3' charges are $(5/3, 2/3, -1/3; 2/3)$.

Pairs of colored technipions will be produced with substantial cross sections at supercollider energies, principally by gluon fusion. As an example, I show in Figure 29 the integrated cross section for the reaction

$$p p \rightarrow P_3 \bar{P}_3 + \text{anything} ,\qquad\qquad (98)$$

with and without the technirho $(\rho_8^{0'})$ enhancement. The expected decay modes of the color-triplet technipions are

$$P_3 \rightarrow q\bar{\ell} \text{ or } \bar{q}\bar{q} ,\qquad\qquad (99)$$

i.e., final states such as $t\tau^+, t\nu_\tau, b\tau^+, \bar{t}\bar{b}$, etc. Production rates are substantial; the challenge will be to identify and measure the heavy-fermion decay products.

If the technicolor hypothesis correctly describes the breakdown of the electroweak gauge symmetry, there will be a number of spinless technipions with masses below the technicolor scale of about 1 TeV. In the simplest versions of technicolor, some of these—the color singlet, technicolor singlet particles—should be quite light (with masses $\lesssim 40$ GeV/c^2) and could be studied using the current generation of e^+e^- and $\bar{p}p$ colliders. Similar light scalars arise in multiple Higgs models and in supersymmetry. With plausible assumptions for the principal decay modes, searches for charged scalars in Z^0 decay at LEP[71] exclude technipions with masses less than about 35 GeV/c^2. The colored technipions are probably inaccessible to experiment before a supercollider comes into operation, as are the technivector mesons. Full exploitation of the scientific opportunities requires the efficient identification and measurement of heavy quark flavors and—for the technivector mesons—the ability to identify intermediate bosons in complex events.

One of the vulnerabilities of technicolor models is that they do not naturally guarantee the absence of flavor-changing neutral currents. In "walking technicolor" models,[72] in which the $SU(N)_{TC}$ coupling evolves very slowly over a large range of momenta above Λ_{TC}, it appears possible to suppress flavor-changing neutral currents. A secondary consequence would be to increase the masses of the lightest technipions to about 100 GeV/c^2.

TOWARD THE FRONTIER

In these lectures, I have indicated why we believe the standard model must be incomplete and why its shortcomings identify the 1-TeV scale as the regime in which definitive clues about the nature of electroweak symmetry breaking are to be found. The incompleteness of our theoretical description is manifested by our ignorance of the dynamical mechanism that underlies the spontaneous breaking of the electroweak gauge symmetry, by the multitude of seemingly arbitrary parameters required to specify the standard model, by the puzzling replication of quark and lepton generations, and by many other questions. For example, we do not know whether additional fundamental forces and elementary constituents remain to be discovered, nor do we understand how—or whether—the fundamental interactions can be unified.

I have also introduced the hadron colliders that we hope will open this high-energy frontier and sketched some of the challenges of a high-energy, high-luminosity experimental environment. In this brief survey, it has been possible only to scratch the surface of the physics opportunities presented by a hadron supercollider. A supercollider should provide the means to test thoroughly the predictions of the standard model, to illuminate the physics of electroweak symmetry breaking, and to explore the unknown. The examples we have considered indicate the scope of physics issues to be addressed, from detailed study of known particles to the search for high-mass exotica.

REFERENCES

1. E. Eichten, I. Hinchliffe, K. D. Lane, and C. Quigg, *Rev. Mod. Phys.* 56,
   579 (1984); ibid. 58, 1065E (1986).
2. *Proceedings of the 1984 Summer Study on Design and Utilization of the
   Superconducting Super Collider*, edited by R. Donaldson and J. G. Morfín
   (Fermilab, Batavia, Illinois, 1984).
3. *p̄p Options for the Supercollider*, edited by J. E. Pilcher and A. R. White
   (University of Chicago, 1984).
4. *Physics at the Superconducting Super Collider Summary Report*, edited
   by P. Hale and B. Winstein (Fermilab, 1984).
5. *Large Hadron Collider in the LEP Tunnel*, edited by G. Brianti, et al.,
   CERN 84-10.
6. *Supercollider Physics*, edited by D. E. Soper (World Scientific, Singa-
   pore, 1986).
7. *Proceedings of the Summer Study on the Physics of the Superconducting
   Super Collider, Snowmass, 1986*, edited by R. Donaldson and J. Marx (Di-
   vision of Particles and Fields of the American Physical Society, New
   York, 1987).
8. *The Large Hadron Collider in the LEP Tunnel*, edited by G. Brianti and
   K. Hübner, CERN 87-05.
9. *Proceedings of the Workshop on Physics at Future Accelerators, La Thuile
   and Geneva*, edited by J. H. Mulvey, CERN 87-07.
10. *Proceedings of the Workshop on Experiments, Detectors, and Experimen-
    tal Areas for the Supercollider*, Berkeley, 1987, edited by R. Donaldson
    and M. G. D. Gilchriese (World Scientific, Singapore, 1988).
11. *The feasibility of experiments at high luminosity at the Large Hadron
    Collider*, edited by J. H. Mulvey, CERN 88-02.
12. *High Energy Physics in the 1990s, Snowmass, 1988*, edited by Sharon
    Jensen (World Scientific, Singapore, 1989).
13. *Proceedings, ECFA study week on instrumentation technology at high-
    luminosity hadron colliders, Barcelona*, edited by E. Fernandez and
    G. Jarlskog, CERN 89-10.

14. The weak-isospin assignment of b is determined by the absence of flavor-changing multilepton decays of b, and by the forward-backward asymmetry measured in the reaction $e^+ e^- \to b \bar{b}$. The necessity of a strong multilepton signal in a five-quark model is explained by G. L. Kane and M. E. Peskin, *Nucl. Phys.* B195, 29 (1982). The current upper limit is $[\Gamma(b \to \mu^+ \mu^- X) + \Gamma(b \to e^+ e^- X)]/\Gamma(b \to all) < 2.4 \cdot 10^{-3}$ (Particle Data Group (M. Aguilar-Benitez, et al.), *Phys. Lett.* B239, 1 (1990)). See H. Sagawa, et al. (AMY collaboration), *Phys. Rev. Lett.* 63, 2341 (1989), for a recent compilation of asymmetry measurements.

15. The inference of an upper bound on the mass of the top quark from the apparent absence of large radiative corrections to the strength of neutral-current interactions is discussed by P. Langacker, in these proceedings.

16. "A new limit on the mass of the top quark," CDF Collaboration, presented by K. Sliwa, Fermilab–CONF–90/93–E; invited talk at XXV Rencontres de Moriond, Les Arcs, Savoie, France, March 4-18, 1990; to appear in the Proceedings. The best published results ($m_t > 77$ GeV/c^2 at 95% CL) are reported in CDF Collaboration (F. Abe, et al.), *Phys. Rev. Lett.* 64, 142, 147 (1990). The CDF top search is described in detail by J. Peoples, these proceedings. A search that does not depend on a specific decay chain has been carried out in the study of Z^0 decays at LEP. The ALEPH collaboration (D. Decamp, et al.), *Phys. Lett.* B236, 511 (1990) reports $m_t > 45.8$ GeV/c^2 at 95% CL.

17. The notation here is that of C. Quigg, *Gauge Theories of the Strong, Weak, and Electromagnetic Interactions* (Addison-Wesley, Reading, Mass., 1983).

18. For a thorough quantitative assessment of the current status of the standard electroweak model, see P. Langacker, these proceedings.

19. A single, distinct particle is only the simplest example of a direct-channel singularity canceling the residual divergence in the amplitude. The possibility that there might be no recognizable Higgs boson is emphasized by M. S. Chanowitz, these proceedings.

20. A. D. Linde, *Pis'ma Zh. Eksp. Teor. Fiz.* 23, 73 (1976) [*JETP Lett.* 23, 64 (1976)]; S. Weinberg, *Phys. Rev. Lett.* 36, 294 (1976).

21. Manfred Lindner, Marc Sher, and Helmut W. Zaglauer, *Phys. Lett.* B228, 139 (1989). For a review of electroweak Higgs potentials and vacuum stability, see M. Sher, *Phys. Rep.* 179, 273 (1989).

22. The classic application to the reaction $\nu_\mu e \to \mu \nu_e$ is presented in T. D. Lee and C.-S. Wu, *Ann. Rev. Nucl. Sci.* 15, 381 (1965).

23. B. W. Lee, C. Quigg, and H. B. Thacker, *Phys. Rev. Lett.* 38, 883 (1977); *Phys. Rev.* D16, 1519 (1977).

24. R. Dashen and H. Neuberger, *Phys. Rev. Lett.* 50, 1897 (1983); M. P. Lüscher and P. Weisz, *Nucl. Phys.* B318, 705 (1989); J. Kuti, L. Lin, and Y. Shen, *Phys. Rev. Lett.* 61, 678 (1988); G. Bhanot and K. Bitar, ibid. 61, 798 (1988); A. Hasenfratz, et al., *Nucl. Phys.* B317, 81 (1989). Recent reviews are J. Jersák, "Lattice Studies of the Higgs System," Jülich preprint HLRZ–89–45; H. Neuberger, "Higgs Physics on the Lattice," Rutgers preprint RU–89–44.

25. J. Ellis, M. K. Gaillard, and D. Nanopoulos, *Nucl. Phys.* B106, 292 (1976).

26. A. I. Vainshtein, V. I. Zakharov, and M. A. Shifman, *Usp. Nauk Fiz.* **131**, 537 (1980) [English translation: *Sov. Phys.* **23**, 479 (1980)].

27. M. S. Chanowitz, *Ann. Rev. Nucl. Part. Sci.* **38**, 323 (1988).

28. R. N. Cahn, *Rep. Prog. Phys.* **52**, 389 (1989).

29. J. F. Gunion, H. E. Haber, G. L. Kane, and S. Dawson, *The Higgs Hunter's Guide* (Addison-Wesley, Redwood City, California, 1990).

30. C. Quigg, "Hadron Colliders Beyond the Z^0," in *Looking beyond the Z*, Proceedings of the Fifteenth SLAC Summer Institute on Particle Physics, SLAC Report No. 328, edited by Eileen C. Brennan (SLAC, Stanford, California, 1988), p. 179. The unnaturalness of the standard model is defined precisely by G. 't Hooft, in *Recent Developments in Gauge Theories*, proceedings of the 1979 NATO Advanced Study Institute, Cargèse, edited by G. 't Hooft, et al. (Plenum, New York, 1980), p. 135.

31. M. Veltman, *Acta Phys. Pol.* **B12**, 437 (1981); C. H. Llewellyn Smith, *Phys. Rep.* **105**, 53 (1984).

32. L. R. Cormell and G. P. Yost, "Accelerator Parameters Relevant to Detector Design," SSCL–264 (1990, unpublished).

33. G. Brianti, "The large hadron collider (LHC) in the LEP tunnel," CERN/AC/FA 90–03.

34. F. E. Close, *An Introduction to Quarks and Partons* (Academic, New York, 1979); J. L. Rosner, "Quark Models," in *Techniques and Concepts of High Energy Physics*, St. Croix, 1980, edited by T. Ferbel (Plenum, New York, 1981), p. 1; C. Quigg, "Models for Hadrons," lectures given at l'Ecole d'Eté de Physique Théorique, Les Houches, in *Gauge Theories in High Energy Physics*, edited by M. K. Gaillard and R. Stora (North-Holland, Amsterdam, 1983), p. 645.

35. G. Altarelli and G. Parisi, *Nucl. Phys.* **B126**, 298 (1977).

36. The standard form of the Altarelli-Parisi equations and the Mellin transform method of solution in terms of moments of the parton distributions are treated in Quigg, Ref. 30, §8.5. A technique with better convergence properties follows from applying the Altarelli-Parisi strategy to x times the parton distributions; this is used and explained in Ref. 1.

37. H. Abramowicz, et al., *Z. Phys.* **C13**, 199 (1982); **C17**, 283 (1983).

38. *Proceedings of the Workshop on Hadron Structure Functions and Parton Distributions*, edited by D. Geesaman, Jorge Morfín, Cynthia Sazama, and Wu-Ki Tung (World Scientific, Singapore, to be published).

39. R. N. Cahn and Sally Dawson, *Phys. Lett.* **136B**, 196 (1984); ibid., **138B**, 464E (1984).

40. Michael S. Chanowitz and Mary K. Gaillard, *Phys. Lett.* **142B**, 85 (1984).

41. S. Dawson, *Nucl. Phys.* **B249**, 42 (1985).

42. G. L. Kane, W. W. Repko, and W. B. Rolnick, *Phys. Lett.* **148B**, 367 (1984).

43. M. S. Chanowitz and Mary K. Gaillard, *Nucl. Phys.* **B261**, 379 (1985).

44. R. N. Cahn, *Nucl. Phys.* **B255**, 341 (1985); ibid., **B262**, 744E (1985).

45. M. D. Marx, et al., *EMPACT (Electrons, Muons, Partons with Air-Core Toroids) Collaboration Expression of Interest* (May 1990).

46. S. C. C. Ting, et al., *L* Collaboration Expression of Interest* (May 1990).

47. G. H. Trilling, et al., *Solenoidal Detector Collaboration Expression of Interest* (May 1990).

48. Ian Hinchliffe, "Trigger Rates at SSC," LBL Report SSC-SDE-3 (June 20, 1989, unpublished).

49. J. Peoples, these proceedings.

50. F. Abe, et al. (CDF collaboration), *Phys. Rev. Lett.* **63**, 720 (1989). See also M. Campbell, "Electroweak Results from CDF," in *Proceedings of the 1989 International Symposium on Lepton and Photon Interactions at High Energies*, edited by M. Riordan (World Scientific, Singapore, 1990), p. 274.

51. Preliminary results on the reconstruction of B-mesons are reported in the talk by D. Baden at the 1990 SLAC Summer Institute.

52. For a recent example, see F. Abe, et al. (CDF collaboration), *Phys. Rev. Lett.* **62**, 3020 (1989).

53. E. Eichten, K. Lane, and M. E. Peskin, *Phys. Rev. Lett.* **50**, 811 (1983).

54. F. Abe, et al. (CDF collaboration), *Phys. Rev. Lett.* **62**, 613 (1989).

55. M. Green and J. Schwarz, *Phys. Lett.* **149B**, 117 (1984); ibid. **151B**, 21 (1985); D. J. Gross, J. A. Harvey, E. Martinec, and R. Rolm, *Phys. Rev. Lett.* **54**, 502 (1985); idem, *Nucl. Phys.* **B256**, 253 (1985); E. Witten, *Nucl. Phys.* **B258**, 75 (1985); M. Dine, V. Kaplunovsky, M. Mangano, C. Nappi, and N. Seiberg, *Nucl. Phys.* **B259**, 519 (1985).

56. P. H. Frampton and S. L. Glashow, *Phys. Lett.* **190B**, 157 (1987); *Phys. Rev. Lett.* **58**, 2168 (1987).

57. Detailed calculations appear in J. Bagger, C. Schmidt, and S. King, *Phys. Rev.* **D37**, 1188 (1988).

58. I. Hinchliffe and C. Quigg, unpublished.

59. C. Albajar, et al. (UA1 collaboration), *Phys. Lett.* **209B**, 127 (1988).

60. B. L. Combridge, *Nucl. Phys.* **B151**, 429 (1979). The radiative corrections, not included in the estimates displayed in Figure 26, have been evaluated by P. Nason, S. Dawson, and R. K. Ellis, *Nucl. Phys.* **B303**, 607 (1988).

61. R. N. Cahn, et al., in *Proceedings of the Workshop on Experiments, Detectors, and Experimental Areas for the Supercollider*, Berkeley, 1987, edited by R. Donaldson and M. G. D. Gilchriese (World Scientific, Singapore, 1988), p. 20.

62. V. L. Ginzburg and L. D. Landau, *Zh. Eksp. Teor. Fiz.* **20**, 1064 (1950).

63. J. Bardeen, L. N. Cooper, and J. R. Schrieffer, *Phys. Rev.* **106**, 162 (1962).

64. Y. Nambu, *Phys. Rev. Lett.* **4**, 380 (1960). Understanding of the pion's origin in the breakdown of chiral symmetry predates QCD.

65. M. Weinstein, *Phys. Rev.* **D8**, 2511 (1973).

66. S. Weinberg, *Phys. Rev.* **D13**, 974 (1976), ibid. **19**, 1277 (1979).

67. L. Susskind, *Phys. Rev.* **D20**, 2619 (1979).

68. S. Dimopoulos and L. Susskind, *Nucl. Phys.* **B155**, 237 (1979).

69. E. Eichten and K. Lane, *Phys. Lett.* **90B**, 125 (1980).

70. E. Farhi and L. Susskind, *Phys. Rev.* **D20**, 3404 (1979).

71. M. Z. Akrawy, et al. (OPAL collaboration), *Phys. Lett.* **B242**, 299 (1990); D. Decamp, et al. (ALEPH collaboration), *Phys. Lett.* **B241**, 623 (1990); P. Abreu, et al. (DELPHI collaboration), "Search for Heavy Charged Scalars in Z^0 Decays," CERN-EP/90-33.

72. T. Appelquist and L. C. R. Wijewardhana, *Phys. Rev. D36*, 568 (1987); for a review, see T. Appelquist, M. Soldate, T. Takeuchi, and L. C. R. Wijewardhana, Yale report YCTP-P19-88, to be published in the Proceedings of the 12th Johns Hopkins Workshop on Current Problems in Particle Theory, Baltimore, June 9–10, 1988; R. Holdom, "Issues in technicolor model building," Santa Barbara preprint NSF-ITP-90-93; Ken-Ichi Aoki, Masako Bando, Katuya Hasebe, Taichiro Kugo, Hajime Nakatani, *Prog. Theor. Phys.* **82**, 1151 (1989); T. Appelquist, "Walking Technicolor," in *New Trends in Strong Coupling Gauge Theories*, edited by M. Bando, T. Muta, K. Yamawaki (World Scientific, Singapore, 1989), p. 34.
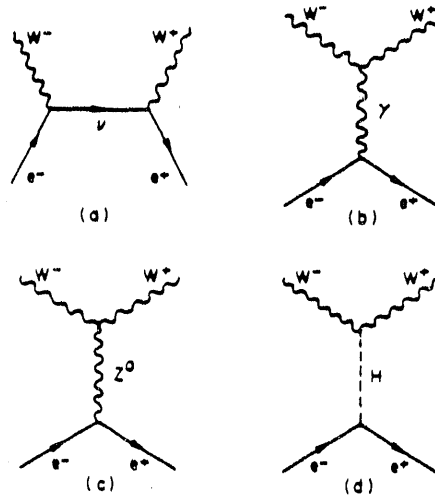
FIGURE 1   Lowest-order contributions to the reaction $e^+e^- \to W^+W^-$ in the standard model.
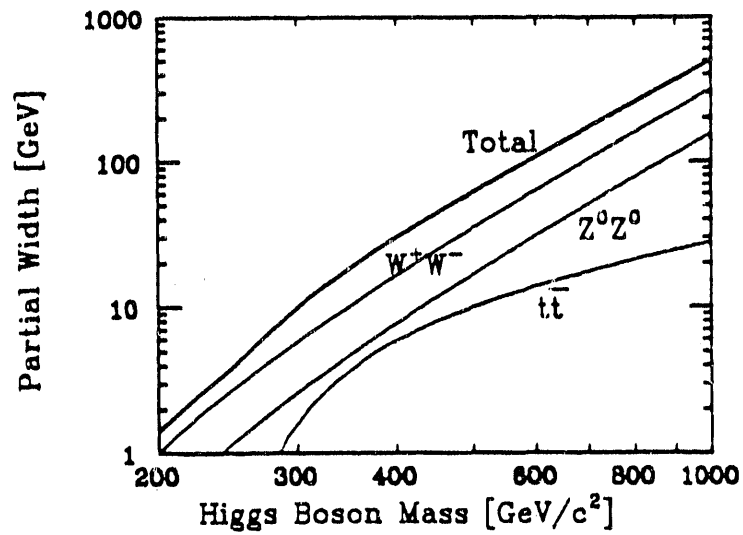
FIGURE 2   Partial decay widths for a heavy Higgs boson in the standard model. The top-quark mass is taken to be 125 GeV/c^2.
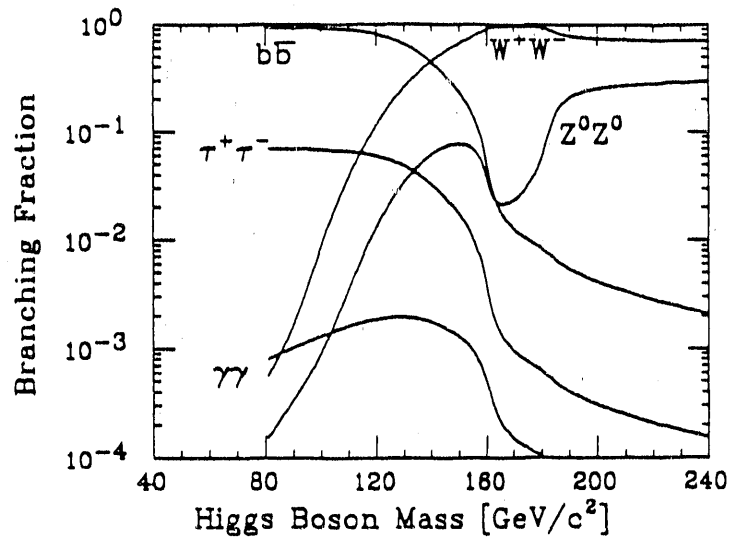
FIGURE 3   Branching fractions for a standard-model Higgs boson of in-
termediate mass, with $m_b = 4.9$ GeV/c^2 and $m_t = 125$ GeV/c^2.
The rate for $H \rightarrow b\bar{b}$ is multiplied by 0.6 to approximate
radiative corrections. The treatment of WW and ZZ below
threshold is due to R. N. Cahn (private communication).
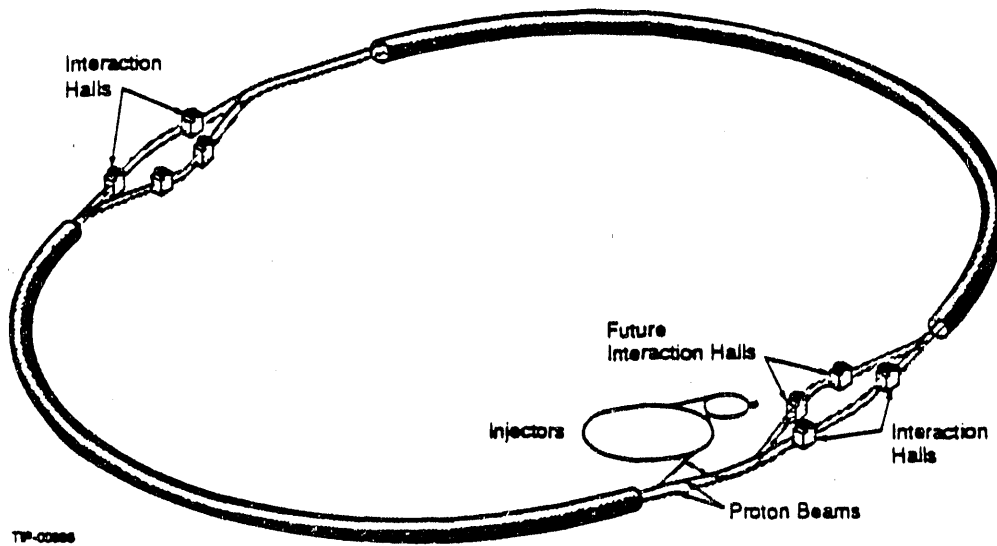
FIGURE 4   The SSC accelerator complex and experimental areas.
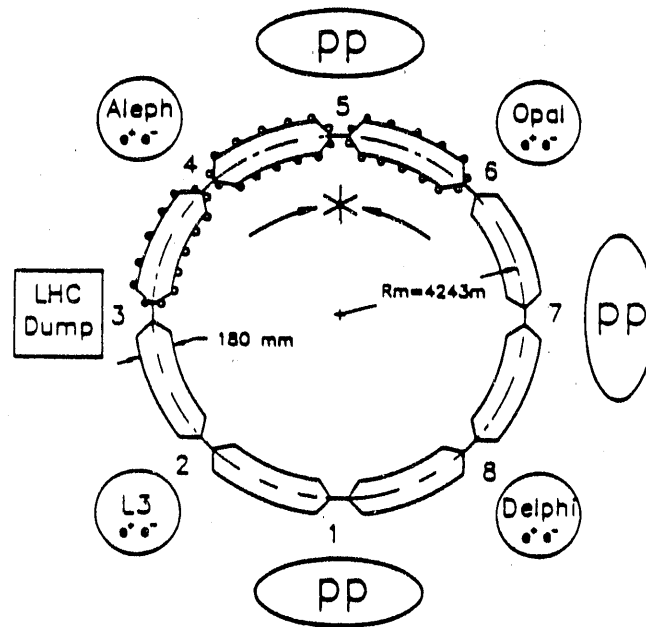
FIGURE 5 Schematic drawing of the Large Hadron Collider in the LEP tunnel.
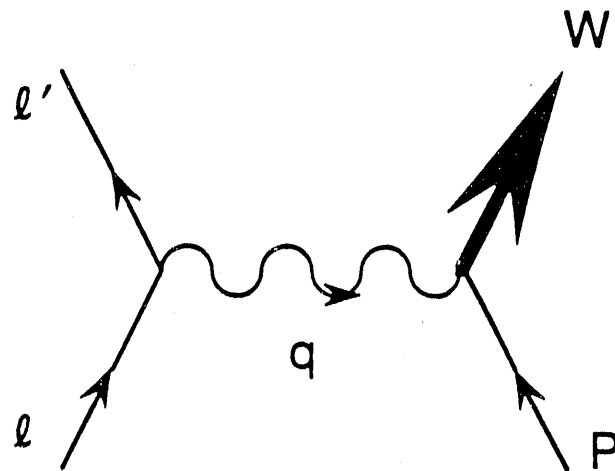
FIGURE 6 Kinematics of deeply inelastic scattering.

C. QUIGG
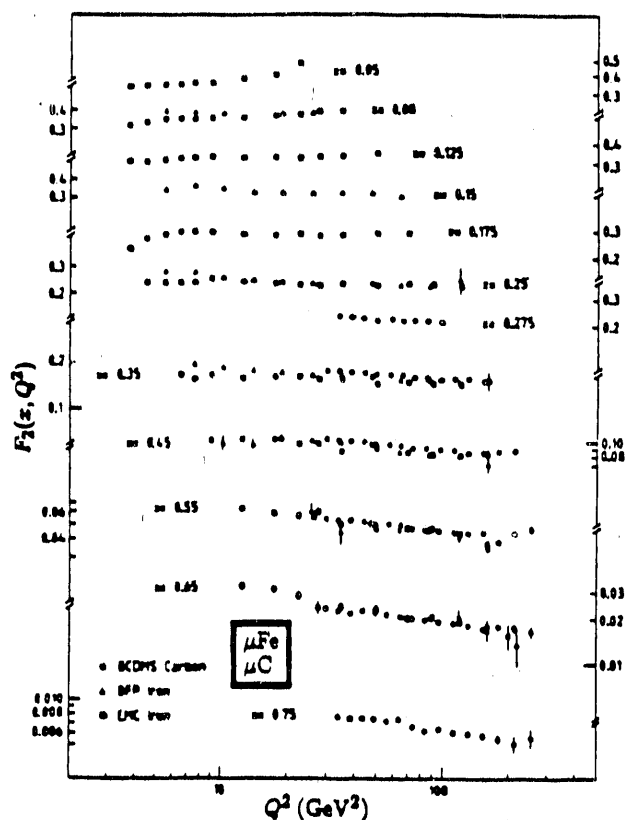
FIGURE 7 The structure function $F_2^{\mu p}(x)$ measured in the scattering of muons on iron (BFP, EMC) and carbon (BCDMS) depends only weakly on the momentum transfer Q^2. The ratio $R = \sigma_L/\sigma_T = 0$ is assumed for the BFP data and a QCD prediction for R is used in the EMC and BCDMS data (from Particle Data Group, Ref. 14).
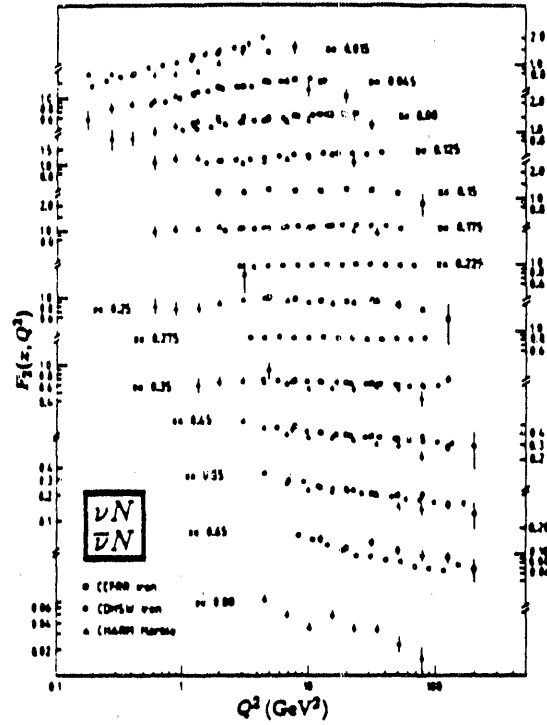
FIGURE 8   The structure function $\mathcal{F}_2^{\nu N}$ measured in neutrino and an-
tineutrino scattering on iron (CCFRR, CDHSW) and marble
(CHARM) targets (from Particle Data Group, Ref. 14). The
ratio of longitudinal to transverse cross sections is taken to be
given by QCD in the CCFRR and CDHSW analyses, and is set
equal to zero in the CHARM analysis.
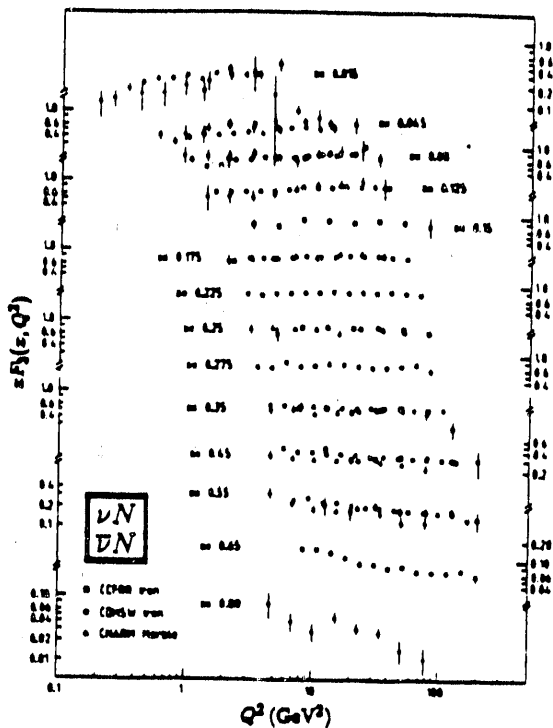
FIGURE 9 The structure function $x\mathcal{F}_3^{\nu N}$ measured in neutrino and antineutrino scattering on iron (CCFRR, CDHSW) and marble (CHARM) targets (from Particle Data Group, Ref. 14). The ratio of longitudinal to transverse cross sections is taken to be given by QCD in the CCFRR and CDHSW analyses, and is set equal to zero in the CHARM analysis.
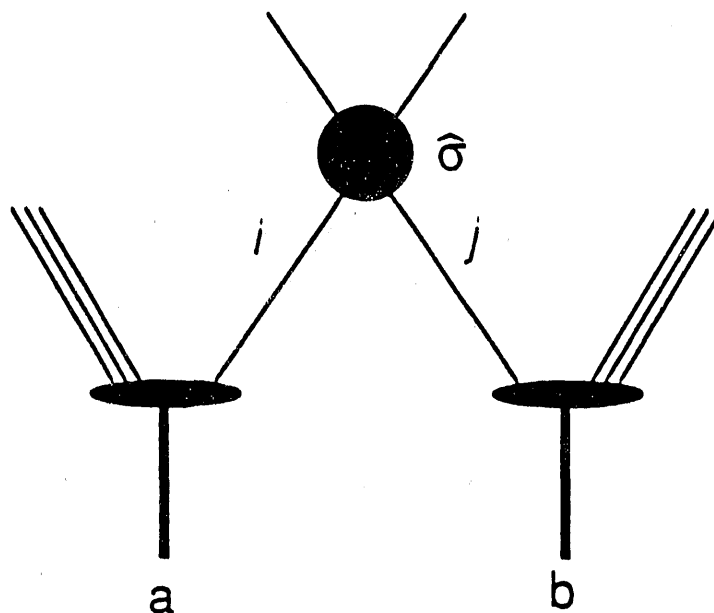
FIGURE 10   Parton-model representation of a hard-scattering event.
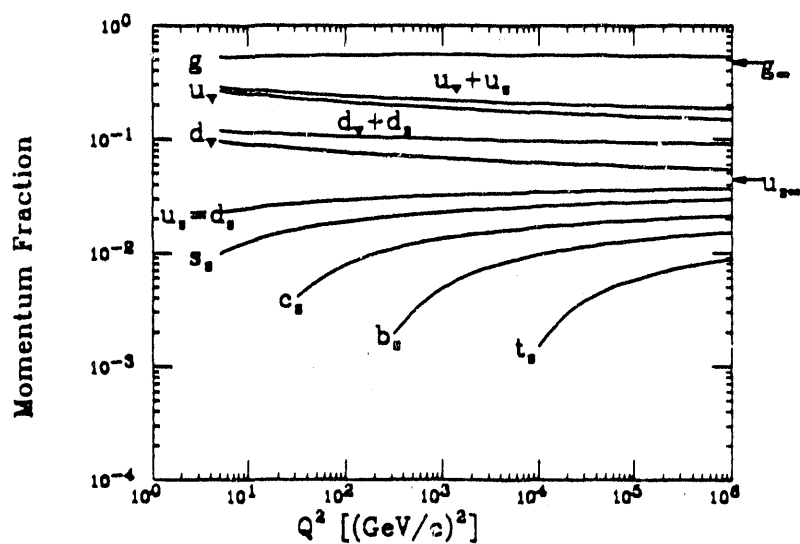
FIGURE 11   Momentum fractions of parton species in Set 2 of the 1986
EHLQ distributions, Ref. 1.
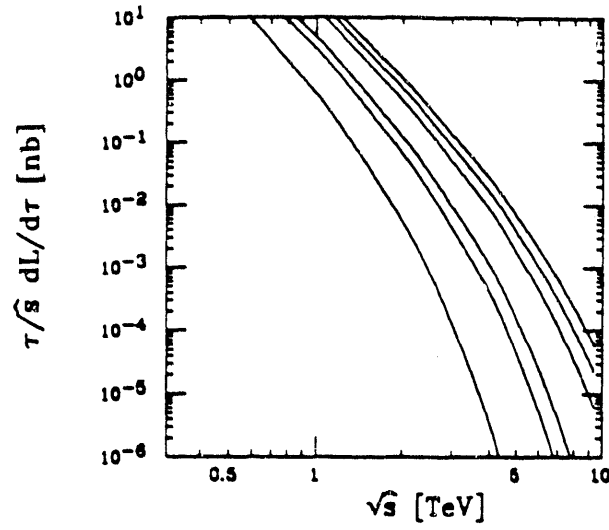
FIGURE 12   The quantity $(\tau/\hat{s})\dfrac{d\mathscr{L}}{d\tau}$ for gg interactions in proton-proton collisions at (left to right) $\sqrt{s} = 10, 17, 20, 30, 35,$ and 40 TeV.
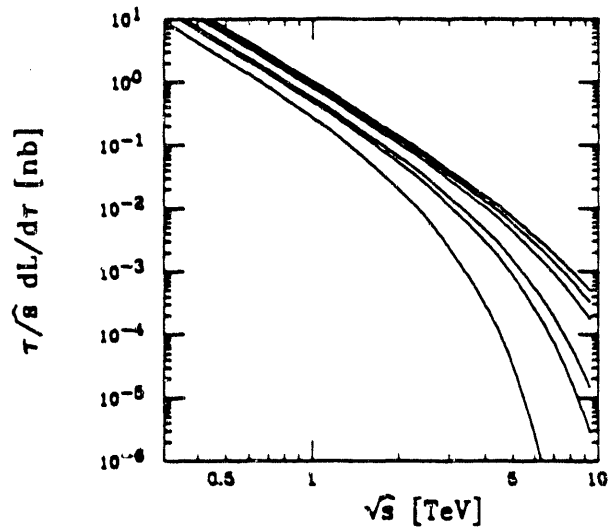
FIGURE 13   The quantity $(\tau/\hat{s})\dfrac{d\mathscr{L}}{d\tau}$ for uu interactions in proton-proton collisions at $\sqrt{s} = 10, 17, 20, 30, 35,$ and 40 TeV.
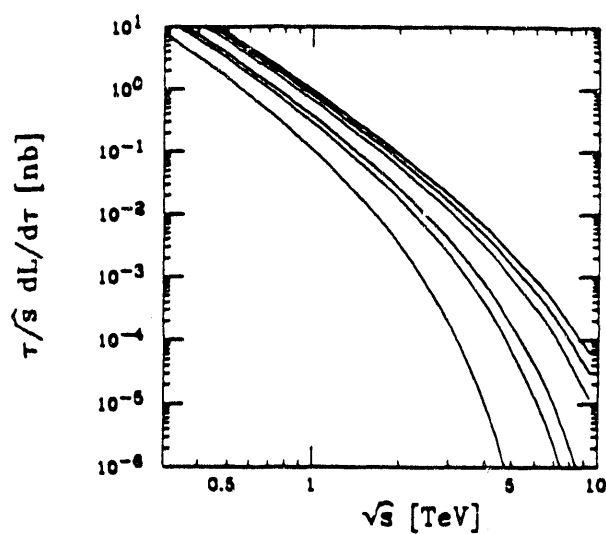
FIGURE 14   The quantity $(\tau/\hat{s})\dfrac{d\mathcal{L}}{d\tau}$ for $u\bar{u}$ interactions in proton-proton collisions at $\sqrt{s} = 10, 17, 20, 30, 35,$ and 40 TeV.
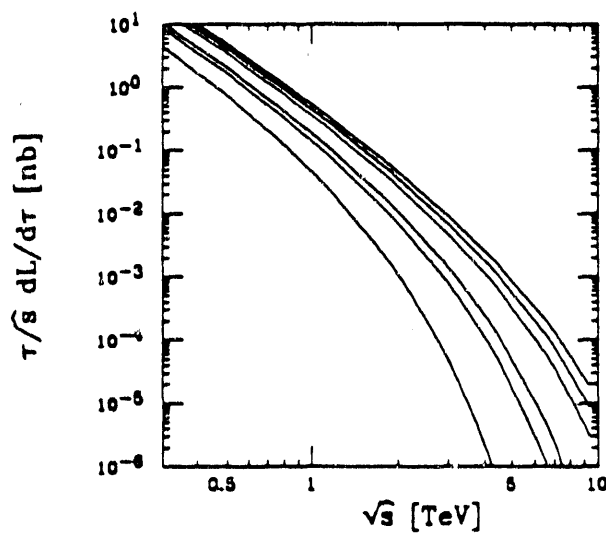
FIGURE 15   The quantity $(\tau/\hat{s})\dfrac{d\mathcal{L}}{d\tau}$ for $d\bar{d}$ interactions in proton-proton collisions at $\sqrt{s} = 10, 17, 20, 30, 35,$ and 40 TeV.
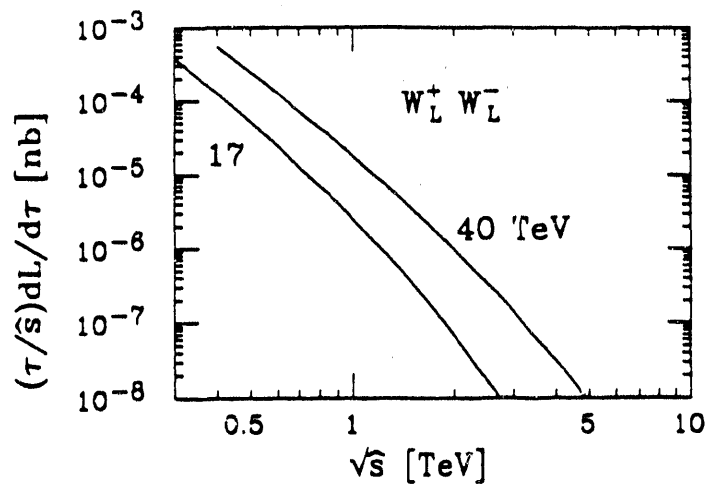
FIGURE 16 The quantity $(\tau/\hat{s})\frac{d\mathcal{L}}{d\tau}$ for $W_L W_L$ interactions in proton-proton collisions at $\sqrt{s} = 17$ and 40 TeV (based on Ref. 41).
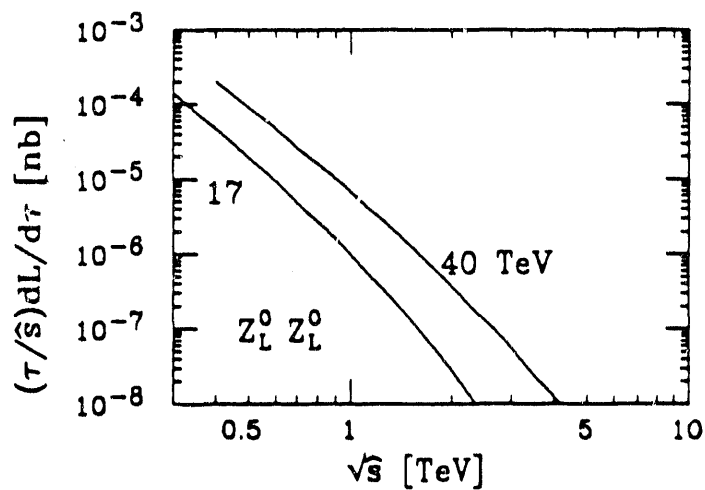
FIGURE 17 The quantity $(\tau/\hat{s})\frac{d\mathcal{L}}{d\tau}$ for $Z_L Z_L$ interactions in proton-proton collisions $\sqrt{s} = 17$ and 40 TeV (based on Ref. 41).
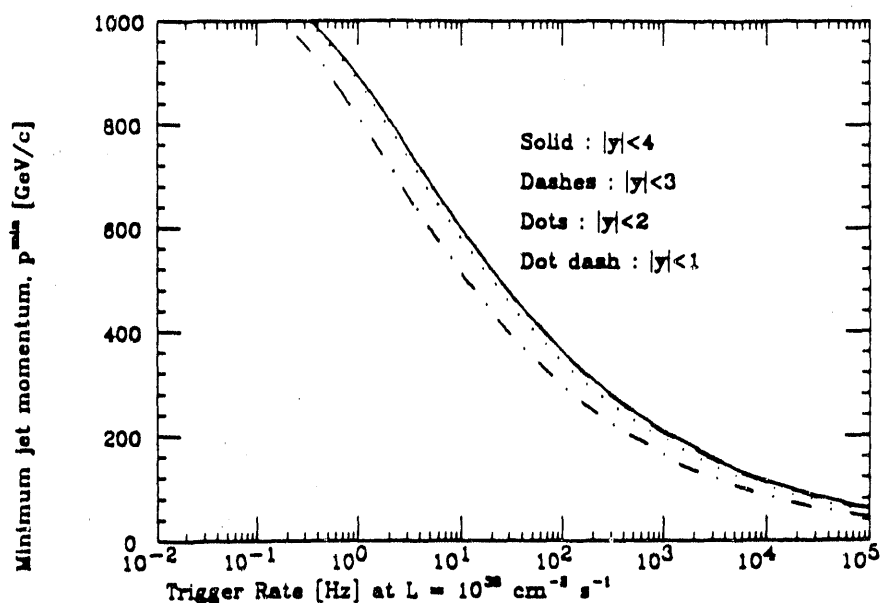
FIGURE 18 Counting rate for a single-jet large-$p_\perp$ trigger in pp collisions at an instantaneous luminosity of $\mathscr{L} = 10^{33} \text{cm}^{-2}\text{sec}^{-1}$. The transverse-momentum threshold is set in the central region, defined by the rapidity cuts indicated (based on Ref. 48).
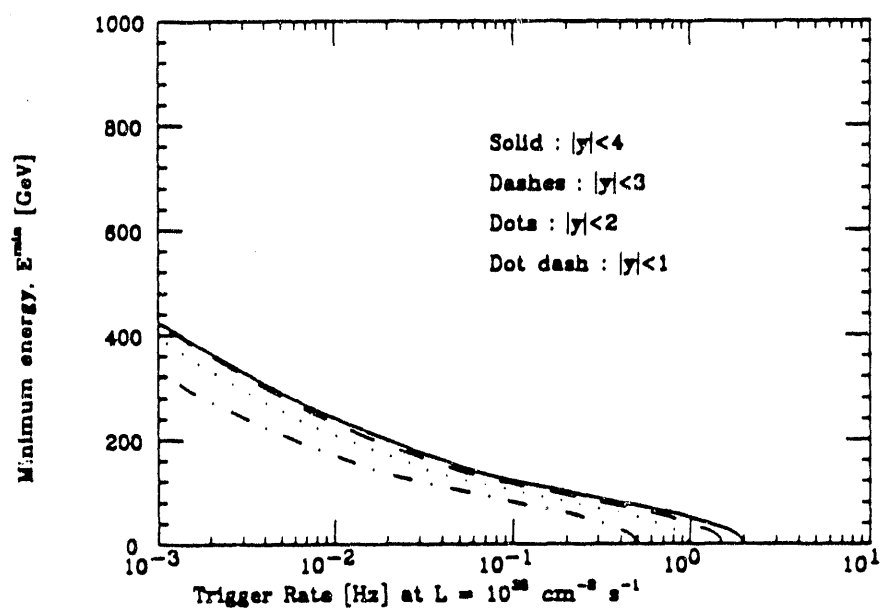
FIGURE 19 Trigger rate (at $\mathscr{L} = 10^{33} \text{cm}^{-2} \text{sec}^{-1}$) for isolated single positrons in 40-TeV pp collisions (based on Ref. 48).

C. QUIGG
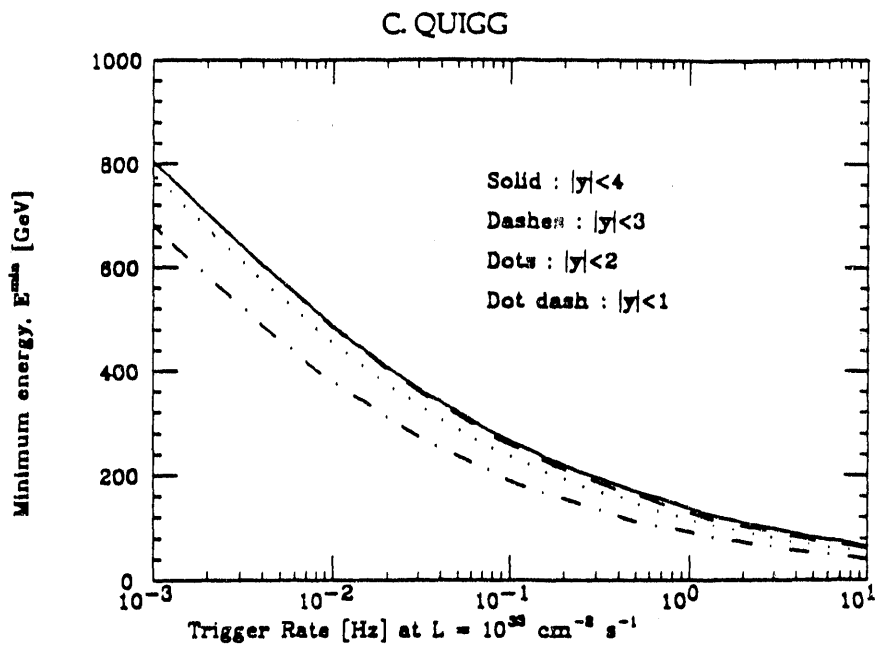
FIGURE 20   Trigger rate (at $\mathscr{L} = 10^{33}$ cm^{-2} sec^{-1}) for isolated single pho-
tons in 40-TeV pp collisions (based on Ref. 48).
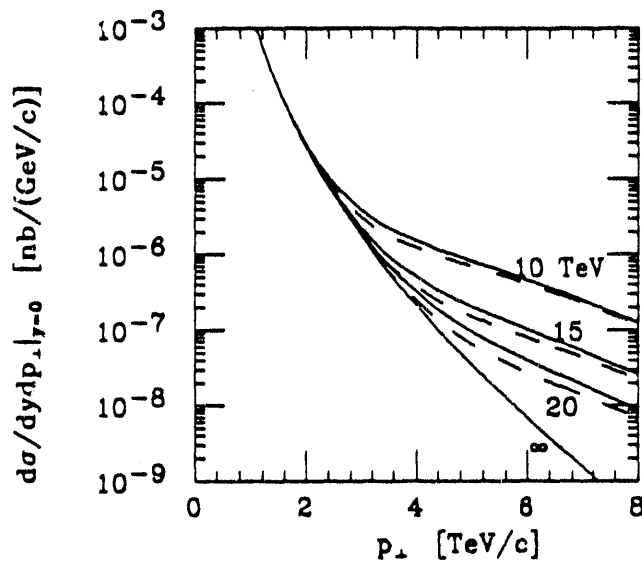
FIGURE 21   Differential cross section $d\sigma/dp_\perp dy\ |_{y=0}$ for the reaction pp
$\rightarrow$ jet + anything at 40 TeV. The curves are labeled by the
compositeness scale Λ^* (in TeV). Solid (dashed) lines indi-
cate constructive (destructive) interference between the QCD
amplitude and the contact term (based on Ref. 1).
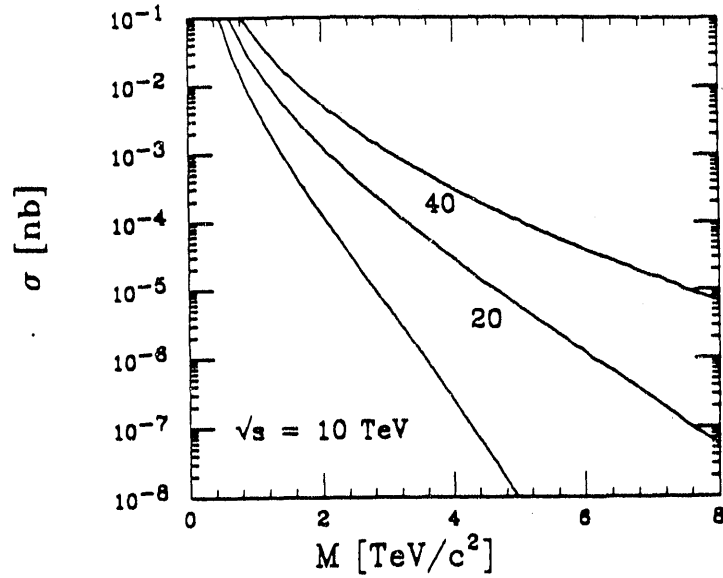
FIGURE 22 Cross section for the production of a heavy W^--boson with rapidity $|y| < 1.5$ in pp collisions at 10, 20, and 40 TeV (based on Ref. 1).
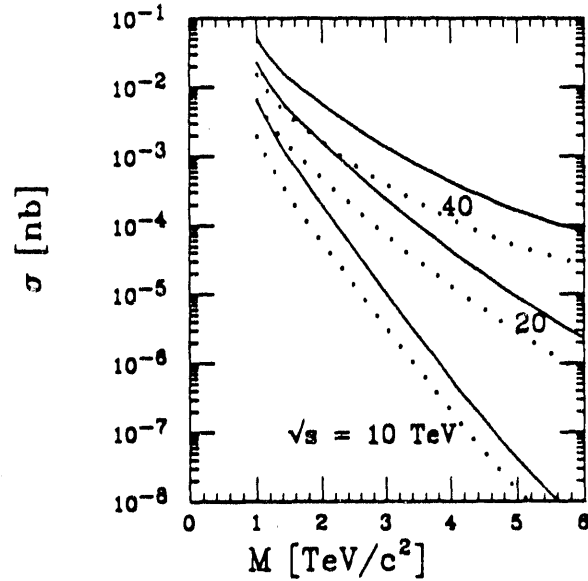
FIGURE 23 Cross section for the production of a heavy $Z^{0\prime}$-boson with rapidity $|y| < 1.5$ in pp collisions at 10, 20, and 40 TeV. Solid lines: Weinberg-Salam couplings; dotted lines: E_6 couplings.
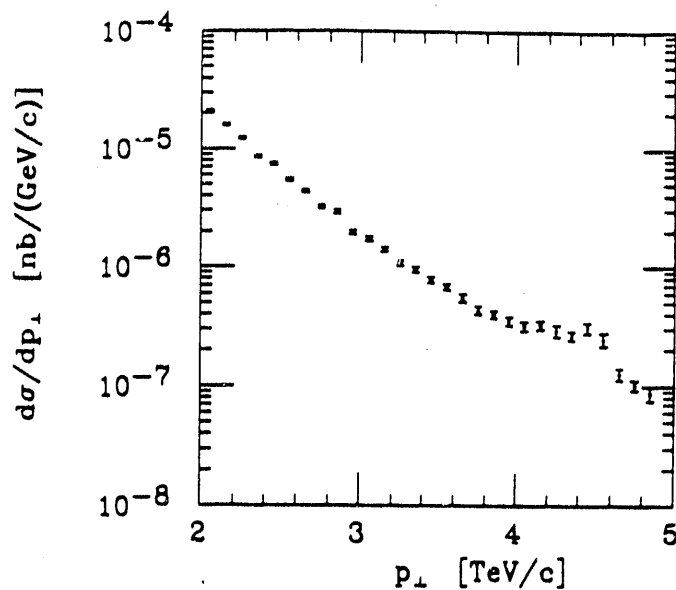
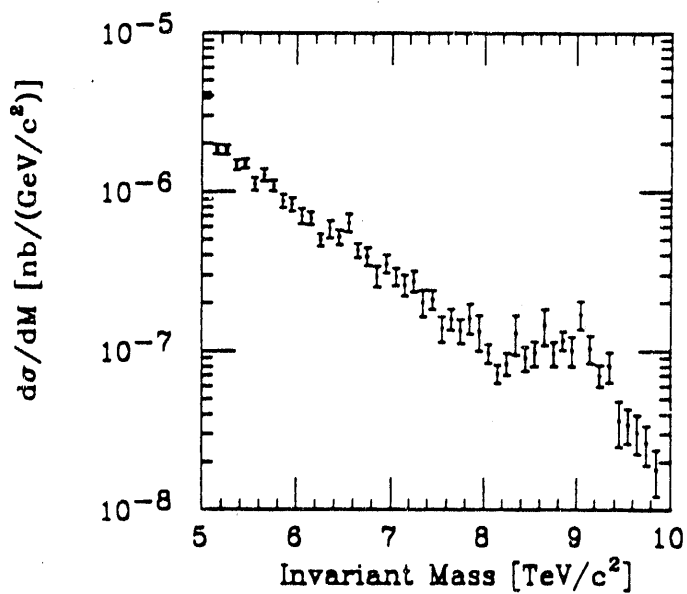FIGURE 24   Cross section $d\sigma/dp_\perp dy$ for $\sqrt{s} = 40$ TeV, including the contribution of a 9-TeV/c^2 axigluon.

FIGURE 25   Invariant mass of a pair of jets produced in pp collisions at $\sqrt{s} = 40$ TeV, including the contribution of a 9-TeV/c^2 axigluon.
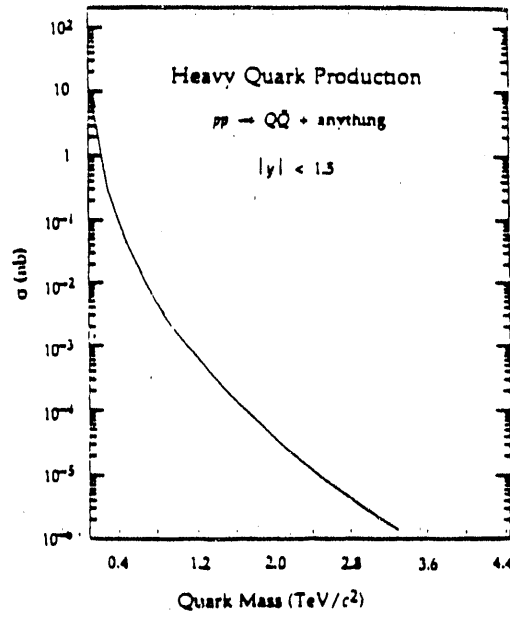
FIGURE 26 Integrated cross section for pair production of heavy quarks
satisfying $|y_Q|$, $|y_{\bar{Q}}| < 1.5$ in pp collisions at 40 TeV (from
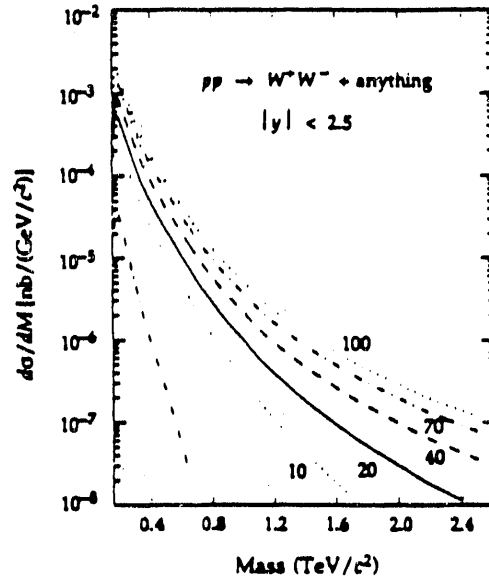Ref. 1).

FIGURE 27 Mass spectrum of W^+W^- pairs produced in pp collisions at
40 TeV, according to the standard model and Set 2 of the
EHLQ parton distributions. Both the W^+ and the W^- must
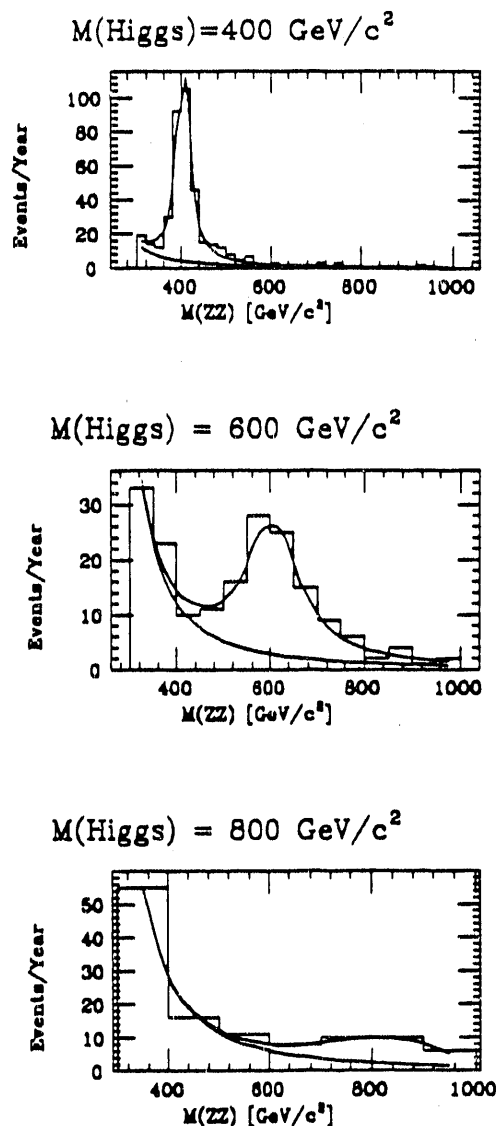satisfy $|y| < 2.5$ (from Ref. 1).

C. QUIGG

M(Higgs)=400 GeV/c^2

M(Higgs) = 600 GeV/c^2

M(Higgs) = 800 GeV/c^2

FIGURE 28 The ZZ invariant mass distribution arising from the produc-
tion and decay of a Higgs boson in the reaction $pp \rightarrow$
H + anything, and from the background process $\bar{q}q \rightarrow ZZ$ at
$\sqrt{s} = 40$ TeV with an integrated luminosity of 10^{40} cm^{-2}. Both
gauge bosons must satisfy the cut $|y| < 1.5$. The top-quark
mass is taken to be 200 GeV/c^2, and perfect resolution and
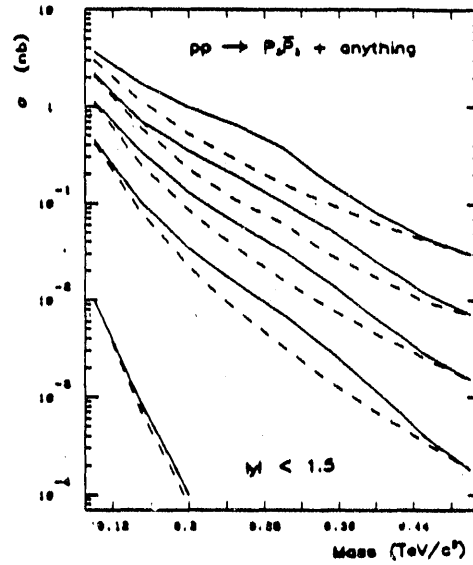detection efficiency is assumed for both electrons and muons
(from Ref. 61).

FIGURE 29 Integrated cross section for the production of $P_3 \bar{P}_3$ pairs in pp
collisions, as a function of the P_3 mass (from Ref. 1).
Rapidities of the technipions must satisfy $|y| < 1.5$. The
cross sections are shown with (solid lines) and without
(dashed lines) the technirho enhancement. The expected
mass of P_3 is around $160 \, \text{GeV}/c^2$.

END

DATE FILMED

12/26/90